



OPEN

Modification of sugarcane bagasse with iron(III) oxide-hydroxide to improve its adsorption property for removing lead(II) ions

Pornsawai Praipipat^{1,2✉}, Pimploy Ngamsurach^{1,2} & Amornrat Sanghuayprai¹

Lead contamination in wastewater results in toxicity of aquatic life and water quality, it is recommended to remove lead before discharging. Four sugarcane bagasse adsorbent materials of sugarcane bagasse powder (SB), sugarcane bagasse powder doped iron(III) oxide-hydroxide (SBF), sugarcane bagasse powder beads (SBB), and sugarcane bagasse powder doped iron(III) oxide-hydroxide beads (SBFB) were synthesized and characterized with various techniques. Their lead removal efficiencies were investigated by batch experiments on the effects of dose (0.1–0.6 g), contact time (1–6 h), pH (1, 3, 5, 7, 9, 11), and concentration (5–30 mg/L), adsorption isotherms, kinetics, and desorption experiments. All materials were amorphous phases presenting specific peaks of cellulose. SBB and SBFB detected sodium alginate peaks, and iron(III) oxide-hydroxide peaks were detected in SBF and SBFB. SB and SBF were scales or overlapping plate surfaces whereas SBB and SBFB had spherical shapes with coarse surfaces. The main functional groups of O–H, C=O, C–H, C–O, and C=C were observed in all materials, whereas Fe–O and –COOH were only found in materials with adding iron(III) oxide-hydroxide or bead material. The point of zero charges (pH_{pzc}) of all materials was higher than 4. The optimum conditions of SB, SBF, SBB, and SBFB with the highest lead removal efficiency at a lead concentration of 10 mg/L and pH 5 were 0.6 g and 6 h (96.08%), 0.2 g and 3 h (100%), 0.2 g and 2 h (98.22%), and 0.1 g and 2 h (100%), respectively. Since SBFB spent less adsorbent dose and contact time than other materials with a lead removal efficiency of 100%, it was a more potential adsorbent than other materials. Thus, adding iron(III) oxide-hydroxide and changing material form helped to improve material efficiencies for lead adsorption. The maximum adsorption capacities of SB, SBF, SBB, and SBFB were 6.161, 27.027, 23.697, and 57.471 mg/L, respectively by fitting the Langmuir model. Langmuir isotherm was best fitted for SB and SBB, whereas the Freundlich model was best fitted for SBF and SBFB. The pseudo-second-order kinetic model was best fitted for all materials. Moreover, all adsorbents could be reused for more than 5 cycles with the lead removal efficiency of more than 73%. Therefore, SBFB was potential material to further apply for lead removal in industrial applications.

The contaminated heavy metals in receiving water are a concern because of their bioaccumulation, persistence, and toxicity to aquatic life and the environment¹. Lead (Pb) is known as the top three most toxic heavy metals followed by mercury (Hg) and cadmium (Cd), and its toxicity creates many human health effects to dysfunction of many human systems such as nerve, blood, tissue, reproductive, digestive, respiratory and many diseases such as anemia, paralysis, barren, and cancer². Increasing lead accumulations in receiving water may be from the discharging of many industries such as batteries, steels, dyes, pigments, and plastics from their manufacturing processes. Therefore, the wastewater with lead contamination is required to remove lead to be below the USEPA water quality standards at 0.05 and 0.2 mg/L for drinking water and industrial wastewater for a safe environment.

Conventional methods of coagulation–flocculation, chemical precipitation, reverse osmosis, membrane filtration, ion exchange, and electrochemical are used for eliminating heavy metals in wastewater; however, these methods have limitations of incomplete heavy metal removals, complicated operations with expensive cost, toxic sludges with requiring disposal³. As a result, many studies attempted to investigate an alternative method with an

¹Department of Environmental Science, Khon Kaen University, Khon Kaen 40002, Thailand. ²Environmental Applications of Recycled and Natural Materials (EARN) Laboratory, Khon Kaen University, Khon Kaen 40002, Thailand. ✉email: pornprai@kku.ac.th

effective and environmentally friendly approach to solve this problem. The adsorption method is an interesting choice for heavy metal removals because it is an effective and eco-friendly method, easy operation, low operation cost, and low creation of sludge after treatment⁴. In addition, various adsorbents such as activated carbon, chitosan, zeolite, silica, resin, nanocomposite, tomato peels, shrimp shells, coconut shells or husk, oil palm shells, banana peels, corn stalk, rice husk, sawdust, bagasse, bagasse fly ash are available choices for eliminating specific target metal ions in wastewater^{5–8}. However, this study will focus on agricultural wastes because of their benefits as low-cost adsorbents used for improving water quality along with reducing waste volumes in terms of waste management. Table 1 demonstrated the elimination of heavy metals from wastewater from various agricultural wastes of sugarcane bagasse, rice straw, coconut, corn, peanut, and sawdust. For sugarcane bagasse, it has been used for removing various heavy metals of lead (Pb), nickel (Ni), chromium (Cr), and copper (Cu) by using unmodified or modified sugarcane bagasse by a hydrothermal method for producing biochar or the addition of zinc chloride (ZnCl₂) into activated carbon^{9–12}. In addition, unmodified agave bagasse has been used for removing Pb(II), cadmium (Cd), and zinc (Zn)¹³. Many previous studies are also used unmodified sugarcane bagasse for removing various heavy metal ions of Pb(II), Ni(II), Cd(II), and Cr(II) in an aqueous solution^{9,14}. Moreover, rice straw modified to biochar with nitro reduction is used for Cd(II) removal¹⁵. For coconut, coconut coir with sodium hydroxide (NaOH) pretreatment is also used for removing Cu(II) while coconut shell was synthesized to activated carbon with lanthanum for Cr(II) removal^{16,17}. The modifications of corncob with xanthate and silica nanocomposite are used for eliminating Pb(II)^{18,19}. Furthermore, the chemical modification of corn husk leaves by bismuthiol I is used for mercury (Hg) removal²⁰. The peanut hull modified with iron chloride and

Adsorbents	Modifications	Metals	Removal efficiency	q_m (mg/g)	Refs
Sugarcane bagasse	Unmodified	Pb	89.31%	1.61	9
	Unmodified	Ni	96.33%	123.46	9
	Biochar	Pb	75.38%	12.74	10
	ZnCl ₂	Cr	93.61%	277.78	11
	ZnCl ₂ -activated carbon	Pb	99.90%	19.30	12
	ZnCl ₂ -activated carbon	Ni	66.40%	2.99	12
	ZnCl ₂ -activated carbon	Cu	90.00%	13.24	12
Agave agasse	Unmodified	Pb	99.40%	93.14	13
	Unmodified	Cd	90.94%	28.50	13
	Unmodified	Zn	80.79%	24.66	13
Rice straw	Biochar/nitration and nitro reduction	Cd	72.10%	72.50	15
Coconut coir	NaOH	Cu	92.19%	–	16
Coconut shell	Activated carbon/lanthanum	Cr	78.00%	0.01	17
Corncob	Xanthate	Pb	79.94%	124.84	18
	Silica/nanocomposite	Pb	95.50%	11.00	19
Corn husk leaves	Bismuthiol I	Hg	98.50%	726.57	20
Peanut hull	Iron chloride and hexamethylenediamine	Cr	–	142.86	21
Sawdust	Poly(<i>N</i> -acryloyl-L-histidine)	Pb	91.50%	241.80	22
Sawdust	Chitosan nanocomposite beads	Cu	86.20%	7.32	23
Sawdust	Chitosan nanocomposite beads	Ni	82.84%	6.92	23
Paddy husk	Biochar	Pb	–	14.20	24
	Biochar	Cu	–	10.27	24
	Biochar	Zn	–	6.48	24
Rice husk	Iron oxide	As	95.00%	82.00	25
	MgAl-layered double hydroxide	Cd	–	113.99	26
	MgAl-layered double hydroxide	Cu	–	101.29	26
Corncob	Aluminium-manganese	Cd	–	45.58	27
	Cerium oxide/nanocomposite	Cd	95.00%	–	28
	Cerium oxide/nanocomposite	Cr	88.00%	–	28
Oil palm bagasse	Al ₂ O ₃ nanoparticles	Cd	87.00%	–	29
	Al ₂ O ₃ nanoparticles	Ni	81.00%	–	29
Peanut shell	Fe ₃ O ₄	Pb	–	188.68	30
<i>Tectona grandis</i> sawdust	Activated carbon modified with iron	As	75.00%	0.68	31
	Activated carbon modified with iron and zirconium	As	86.35%	1.21	31
<i>Lonicera japonica</i> flower	Biomass modified with iron oxide	Pb	–	14.49–23.26	32
		Cu	–	22.73–26.32	32
		Co	–	29.41–50.00	32

Table 1. The elimination of heavy metals from wastewater from various agriculture wastes.

hexamethylenediamine could be used for Cr(II) removal²¹. For sawdust, various heavy metals of Pb(II), Cu(II), and Ni(II) are removed by sawdust modifications by poly (*N*-acryloyl-L-histidine) and chitosan nanocomposite beads^{22,23}. For paddy husk, it is used for producing biochar for Pb(II), Cu(II), and Zn(II) removals²⁴. Among those adsorbents, since bagasse has been popularly used for removing heavy metals in wastewater because of the good chemical properties of cellulose, hemicellulose, lignin, carboxyl, or hydroxyl groups, it is a good choice for lead removal in wastewater. In addition, using sugarcane bagasse can reduce a huge of sugar factory waste along with using these wastes for improving water quality which is a valuable use of resources in an environmental aspect. Although sugarcane bagasse has good chemical properties for removing lead in an aqueous solution, the material improvement method needs to investigate for increasing lead removal efficiency in case of high-strength lead concentration in industrial applications.

Many studies reported using various metal oxides of titanium dioxide (TiO₂), zinc oxide (ZnO), aluminum oxide (Al₂O₃), magnesium oxide (MgO), and iron(II, III) oxide (Fe₃O₄ or Fe₂O₃) have been used to improve adsorbent efficiency by increasing surface area and adsorption capacity and giving fast reaction for heavy metal removals. In Table 1, various agriculture wastes modified with metal oxides have been used for removing heavy metals. For rice husk, the previous studies have been modified by iron oxide and MgAl-layered double hydroxide for removing arsenic (As), Cd(II), and Cu(II)^{25,26}. Various modifications of corncob by aluminum-manganese and cerium oxide nanocomposite for Cd(II) and Cr(II) removals^{27,28}. For oil palm bagasse, it has been modified by aluminum oxide (Al₂O₃) for eliminating Cd(II) and (Ni)²⁹. In addition, the peanut shell was modified with iron(II, III) oxide (Fe₃O₄) for Pb(II) removal³⁰. Sawdust is also used for producing activated carbon and modified with iron (Fe) and zirconium (Zr) for eliminating As(II)³¹. Furthermore, *Lonicera japonica* flower has been studied for producing biomass modified with iron oxide for Pb(II), Cu(II), and cobalt (Co) removals³². Among those metals, iron(III) oxide-hydroxide presented high adsorbent efficiency to deal high strength of heavy metals in wastewater³³, so it is a good idea to use it to improve the efficiency of sugarcane bagasse for lead adsorption in an aqueous solution. In addition, the modification method of stable material is another point to consider for real industrial applications. However, no one modified sugarcane bagasse by changing material form or adding metal oxide, or both to improve material efficiency for lead adsorption in an aqueous solution. Therefore, this study attempts to synthesize sugarcane bagasse adsorbent materials modified with iron(III) oxide-hydroxide in powder and bead materials, compare their lead removal efficiencies through batch experiments, and verify whether adding metal oxide or changing form helped to improve material efficiency for lead adsorption.

The study aimed to synthesize four types of adsorbent materials which were sugarcane bagasse powder (SB), sugarcane bagasse powder doped iron(III) oxide-hydroxide (SBF), sugarcane bagasse beads (SBB), and sugarcane bagasse powder doped iron(III) oxide-hydroxide beads (SBFB). Several characterized techniques of X-Ray Diffractometer (XRD), Field Emission Scanning Electron Microscopy and Focus Ion Beam (FESEM-FIB) with Energy Dispersive X-Ray Spectrometer (EDX), and Fourier Transform Infrared Spectroscopy (FT-IR) were used to investigate their crystalline formations, surface morphologies, chemical compositions, and chemical functional groups. In addition, the point of zero charges (pH_{pzc}) of all materials was studied to identify which pH value had the highest lead removal efficiency. Their lead removal efficiencies were also examined by batch experiments with varying doses, contact time, pH, and concentration. Moreover, their lead adsorption pattern and mechanisms were studied by linear and nonlinear adsorption isotherms of Langmuir, Freundlich, Temkin, and Dubinin–Radushkevich models and kinetics of pseudo-first-order, pseudo-second-order, elovich, and intraparticle diffusion models. Finally, the desorption experiments were investigated to confirm the reusability of the materials.

Result and discussion

The physical characteristics of sugarcane bagasse adsorbent materials. The physical characteristics of SB, SBF, SBB, and SBFB are demonstrated in Fig. 1a–d. For a powder form, SB was yellow color powder shown in Fig. 1a, whereas SBF was brown color powder shown in Fig. 1b. For a bead form, SBB was yellow color beads which had the same color as SB shown in Fig. 1c, whereas SBFB was iron-rust color beads which had a darker brown color than SBF shown in Fig. 1d.

Characterizations of sugarcane bagasse adsorbent materials. *The crystalline patterns of sugarcane bagasse adsorbent materials.* The crystalline formations of SB, SBF, SBB, and SBFB were determined by XRD analysis, and their XRD patterns are presented in Fig. 2a–d. They were amorphous phases with presenting specific peaks of cellulose at 14.48°, 16.66°, 22.36°, and 35.24°³⁴. The sodium alginate peaks of 13.54°, 18.38°, 21.82°, and 38.22°³⁵ were detected in SBB and SBFB shown in Fig. 2c,d. In addition, the specific peaks of iron(III) oxide-hydroxide peaks of 21.56°, 33.16°, 36.56°, 41.68°, and 53.32° matched to JCPDS no. 29-0713³⁶ were only found in SBF and SBFB showed in Fig. 2b,d.

The surface morphologies of sugarcane bagasse adsorbent materials. The surface morphologies of SB, SBF, SBB, and SBFB by FESEM-FIB analysis at 500X magnification with 400 μm for a surface and at 150–160X magnification with 1 mm for a bead illustrated in Fig. 3a–f. For SB, its surface was scales or overlapping plates shown in Fig. 3a. For SBF, its surface was similar to SB with having an iron(III) oxide-hydroxide in a hairy rod shape covered on the surface as shown in Fig. 3b. For SBB, it had a spherical shape with a coarse surface at 160X magnification with 1 mm. Its surface was scaly when was zoomed at 500X magnification with 400 μm demonstrated in Fig. 3c,d. Finally, SBFB had a spherical shape with a coarse surface at 150× magnification of 1 mm. Its surface was heterogenous and coarse surface when zoomed at 500× magnification with 400 μm illustrated in Fig. 3e,f.



Figure 1. The physical characteristics of (a) sugarcane bagasse powder (SB), (b) sugarcane bagasse powder doped iron(III) oxide-hydroxide (SBF), (c) sugarcane bagasse powder beads (SBB), and (d) sugarcane bagasse powder doped iron(III) oxide-hydroxide beads (SBFB).

The chemical functional compositions of sugarcane bagasse adsorbent materials. The chemical compositions of SB, SBF, SBB, and SBFB were analyzed by using EDX analysis represented in Table 2. Three main chemical components of carbon (C), oxygen (O), and calcium (Ca) were found in all sugarcane bagasse adsorbent materials. For sodium (Na) and chloride (Cl), they were detected in all sugarcane bagasse adsorbent materials except SB. For iron (Fe), it was observed only in SBF and SBFB with the addition of iron(III) oxide-hydroxide. For SB and SBF, the mass percentages by weight of C and O were decreased when iron(III) oxide-hydroxide was added to SB, whereas the mass percentage by weight of Ca, Na, Cl, and Fe were increased. The increase in those chemical compositions might be from using chemicals in a process of adding iron(III) oxide-hydroxide by ferric chloride hexahydrate ($\text{FeCl}_3 \cdot 6\text{H}_2\text{O}$) and sodium hydroxide (NaOH) similar to a previous study reported³⁷. For SB and SBB, the mass percentage by weight of C and O decreased when it was changed a form from powder form to bead form, whereas the mass percentage by weight of Ca, Na, and Cl were increased. The increase in those chemical compositions might be from using chemicals in a process of bead formation by sodium alginate ($\text{NaC}_6\text{H}_7\text{O}_6$) and calcium chloride (CaCl_2) supported by the previous studies on the effect of bead formation of materials^{38–41}. For SBF and SBFB, the mass percentage by weight of C, O, and Fe were decreased when SBF was changed to bead form which the decreasing of Fe content might be interfered from the bead formation process. While the mass percentage by weight of Ca, Na, and Cl were increased which might be from using chemicals of $\text{NaC}_6\text{H}_7\text{O}_6$ and CaCl_2 in a process of bead formation similar to SBB. Therefore, the addition of iron(III) oxide-hydroxide and changing the material form affected the increase of Ca, Na, Cl, and Fe contents in sugarcane bagasse adsorbent materials.

The chemical functional groups of sugarcane bagasse adsorbent materials. The chemical functional groups of SB, SBF, SBB, and SBFB were examined by FT-IR analysis, and their FT-IR spectra are demonstrated in Fig. 4a–d. Five main chemical function groups of O–H, C=O, C–H, C–O, and C=C were observed in all materials. The carboxyl group (–COOH) of sodium alginate was only detected in bead materials (SBB and SBFB), and Fe–O was only found in materials with adding iron(III) oxide-hydroxide (SBF and SBFB)^{34,42}. For O–H, it represented the stretching of hydroxyl and phenolic groups, and C=O referred to the stretching of the carbonyl bond of

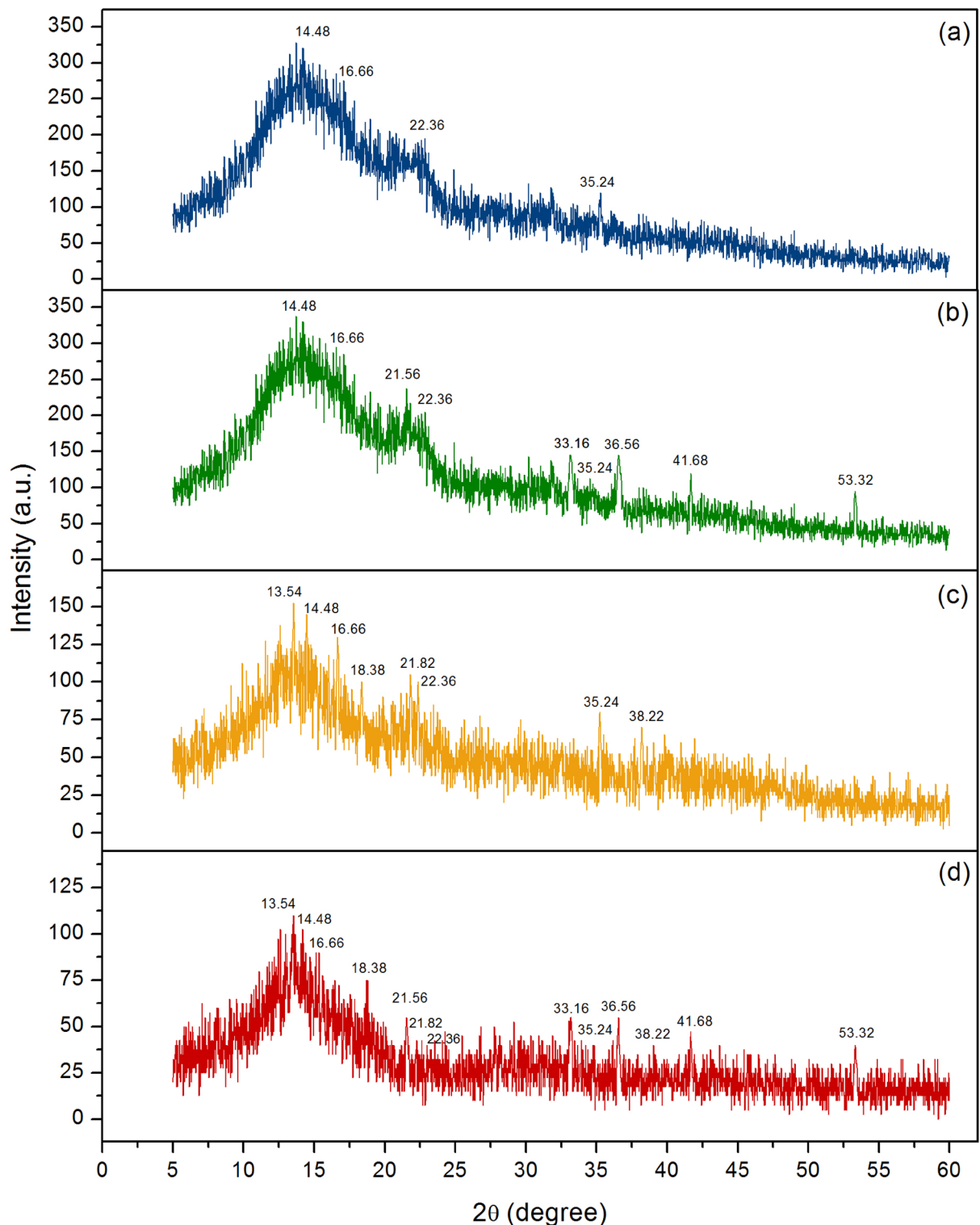


Figure 2. The crystalline patterns of (a) sugarcane bagasse powder (SB), (b) sugarcane bagasse powder doped iron(III) oxide-hydroxide (SBF), (c) sugarcane bagasse powder beads (SBB), and (d) sugarcane bagasse powder doped iron(III) oxide-hydroxide beads (SBFB) by XRD analysis.

hemicellulose and lignin aromatic group in the sugarcane bagasse⁴³. C–H was the stretching of the CH₂ group of cellulose, and C–O was the stretching of alcohol and carboxylic acid⁴⁴. Finally, C=C was the stretching of hemicellulose and cellulose in the sugarcane bagasse³⁴. For SB, the peaks at 3349.84, 1730.39, 1438.70, 1035.43, and 897.32 cm⁻¹ indicated the stretching of O–H, C=O, C–H, C–O, and C=C, respectively shown in Fig. 4a. For

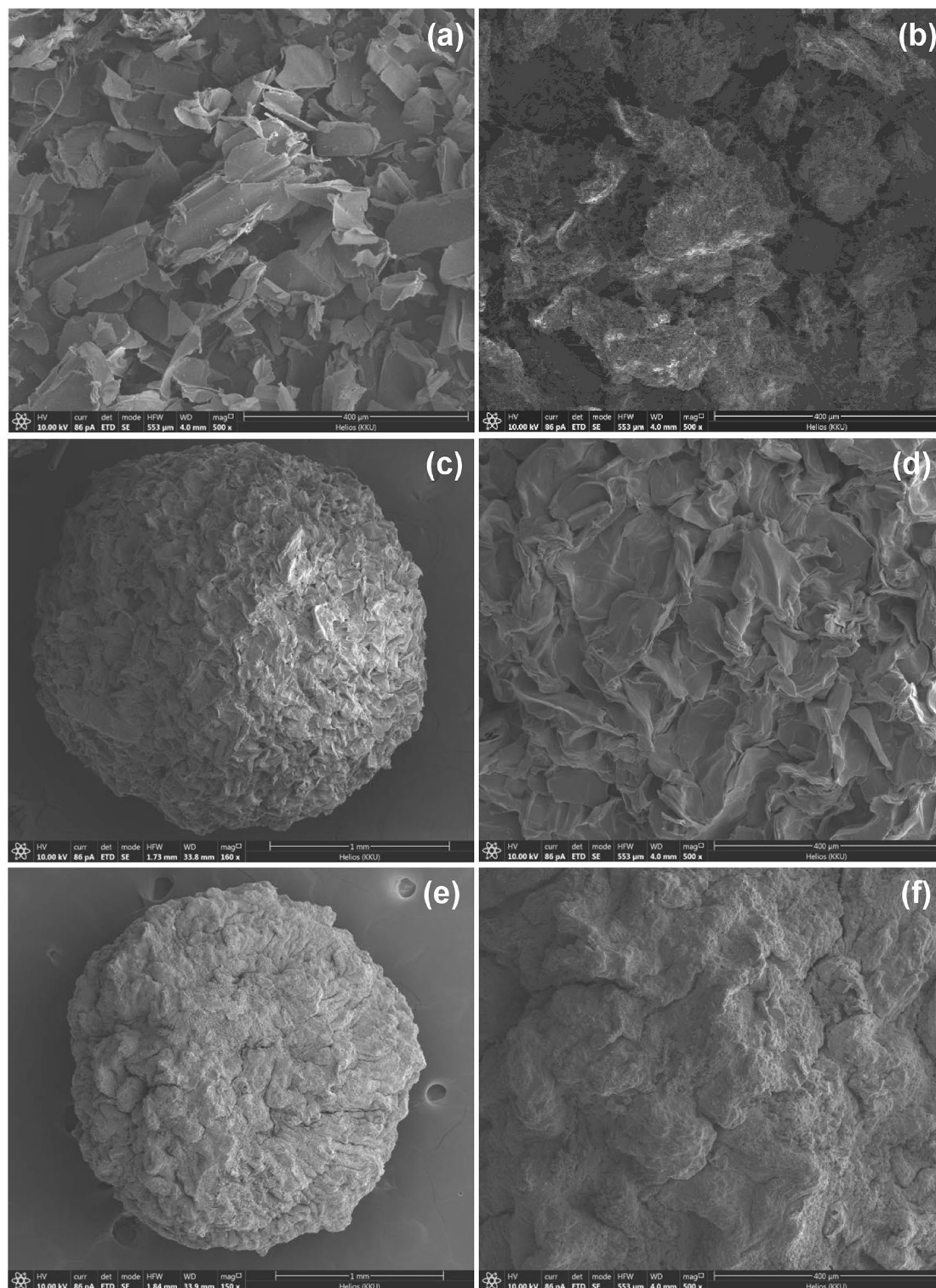


Figure 3. The surface morphologies of (a) sugarcane bagasse powder (SB), (b) sugarcane bagasse powder doped iron(III) oxide-hydroxide (SBF), (c,d) sugarcane bagasse powder beads (SBB) in bead and surface, and (e and f) sugarcane bagasse powder doped iron(III) oxide-hydroxide beads (SBFB) in bead and surface by FESEM-FIB analysis.

SBF, the peaks at 3350.74, 1716.81, 1457.49, 1057.54, 847.21, and 604.93 cm^{-1} represented the stretching of O–H, C=O, C–H, C–O, C=C, and Fe–O, respectively demonstrated in Fig. 4b. For SBB, the peaks at 3316.75, 1737.80, 1591.22, 1421.99, 1026.45, and 883.37 cm^{-1} were the stretching of O–H, C=O, –COOH, C–H, C–O, and C=C,

Chemical compositions (%wt)	Adsorbent materials			
	SB	SBF	SBB	SBFB
C	51.2	41.6	44.7	39.7
O	46.4	44.5	45.8	40.1
Ca	2.4	2.5	8.4	8.6
Na	–	2.1	0.5	2.5
Cl	–	3.0	0.6	3.5
Fe	–	6.3	–	5.6

Table 2. The chemical compositions of sugarcane bagasse powder (SB), sugarcane bagasse powder doped iron(III) oxide-hydroxide (SBF), sugarcane bagasse powder beads (SBB), and sugarcane bagasse powder doped iron(III) oxide-hydroxide beads (SBFB) in the percentages by weight.

respectively illustrated in Fig. 4c. For SBFB, the peaks at 3320.20, 1728.16, 1556.50, 1412.34, 1016.74, 875.11, and 617.20 cm^{-1} referred the stretching of O–H, C=O, –COOH, C–H, C–O, C=C, and Fe–O, respectively shown in Fig. 4d.

The point of zero charges of sugarcane bagasse adsorbent materials. The point of zero charges (pH_{pzc}) of sugarcane bagasse adsorbent materials was studied for determining which pH value of each material is good for lead adsorption. In theory, a pH value that gives the net charge equal to zero is a pH_{pzc} of the adsorbent⁴¹. The pH_{pzc} of SB, SBF, SBB, and SBFB are demonstrated in Fig. 5. The pH_{pzc} of SB, SBF, SBB, and SBFB were 4.33, 4.88, 4.12, and 4.56, respectively, so the addition of iron(III) oxide-hydroxide or the changing material form affected to the increase of pH_{pzc} . The high lead adsorption should happen at the pH of solution higher than the pH_{pzc} ($\text{pH}_{\text{solution}} > \text{pH}_{\text{pzc}}$) of adsorbent because its surface is negatively charged^{33,45}. Therefore, the high lead removal efficiencies of sugarcane adsorbent materials in this study should be found at $\text{pH} > 4$.

Batch adsorption experiments. *The effect of dose.* Six different doses from 0.1 to 0.6 g were used for investigating the dose effect of lead adsorptions by sugarcane bagasse adsorbent materials, and the results are demonstrated in Fig. 6a. The control condition was the lead concentration of 10 mg/L, a sample volume of 200 mL, a contact time of 4 h, pH 5, a temperature of 25 °C, and a shaking speed of 200 rpm. In Fig. 6a, lead removal efficiencies of all materials were increased with the increase of material dose which might be from the increase of surface area or active sites of materials similarly found in previous studies^{33,37,38,45}. The highest lead removal efficiency of SB was 84.29% at 0.6 g whereas the highest lead removal efficiencies of SBF, SBB, and SBFB were 100% at 0.2 g, 0.2 g, and 0.1 g, respectively. Therefore, these were found as the optimum dose of sugarcane bagasse adsorbent materials that were used for studying the contact time effect.

The effect of contact time. The different contact times from 1 to 6 h were used for studying the contact time effect on lead adsorptions by sugarcane bagasse adsorbent materials, and the results are demonstrated in Fig. 6b. The control condition was the lead concentration of 10 mg/L, a sample volume of 200 mL, a temperature of 25 °C, a shaking speed of 200 rpm, and the optimum dose of 0.6 g (SB) or 0.2 g (SBF and SBB) or 0.1 g (SBFB). In Fig. 6b, lead removal efficiencies of all materials were increased with the increase of contact time similar to the dose effect. The highest lead removal efficiency represented the saturated lead adsorption on bagasse adsorbent materials. In Fig. 6b, the highest lead removal efficiency of SB was 96.49% at 6 h whereas the highest lead removal efficiencies of SBF, SBB, and SBFB were 100% at 3 h, 2 h, and 2 h, respectively. Therefore, these were the optimum contact time of sugarcane bagasse adsorbent materials that were used for studying the pH effect.

The effect of pH. The effect of pH was studied by varying pH values of 1, 3, 5, 7, 9, and 11 which represented the acid, neutral, and alkaline conditions on lead adsorptions by sugarcane bagasse adsorbent materials, and the results are demonstrated in Fig. 6c. The control condition was the lead concentration of 10 mg/L, a sample volume of 200 mL, a temperature of 25 °C, a shaking speed of 200 rpm, and the optimum dose of 0.6 g (SB) or 0.2 g (SBF and SBB) or 0.1 g (SBFB) and contact time at 6 h (SB) or 3 h (SBF) or 2 h (SBB and SBFB). In Fig. 6c, lead removal efficiencies of all materials were increased with the increase of pH values from 1 to 7, then they were decreased. The highest lead removal efficiencies of all materials were found at pH 5 with lead removal at 95.88%, 100%, 94.66%, and 100% for SB, SBF, SBB, and SBFB, respectively. This result agreed with the pH_{pzc} results of this study which the pH_{pzc} values of all materials were found at $\text{pH} > 4$. Moreover, it also corresponded to other previous studies that reported the highest lead removal efficiency at $\text{pH} > 4$ relating to pH_{pzc} of lead adsorptions in an aqueous solution^{33,37,45,46}. Therefore, pH 5 was the optimum pH of all sugarcane bagasse adsorbent materials which were used for studying the concentration effect.

The effect of concentration. Several lead concentrations of 5–30 mg/L were used to investigate the concentration effect on lead adsorptions by sugarcane bagasse adsorbent materials, and the results are demonstrated in Fig. 6d. The control condition was a sample volume of 200 mL, a temperature of 25 °C, a shaking speed of 200 rpm, and the optimum dose of 0.6 g (SB) or 0.2 g (SBF and SBB) or 0.1 g (SBFB), contact time at 6 h (SB) or 3 h (SBF) or 2 h (SBB and SBFB), and pH of 5. In Fig. 6d, lead removal efficiencies of all materials were decreased with

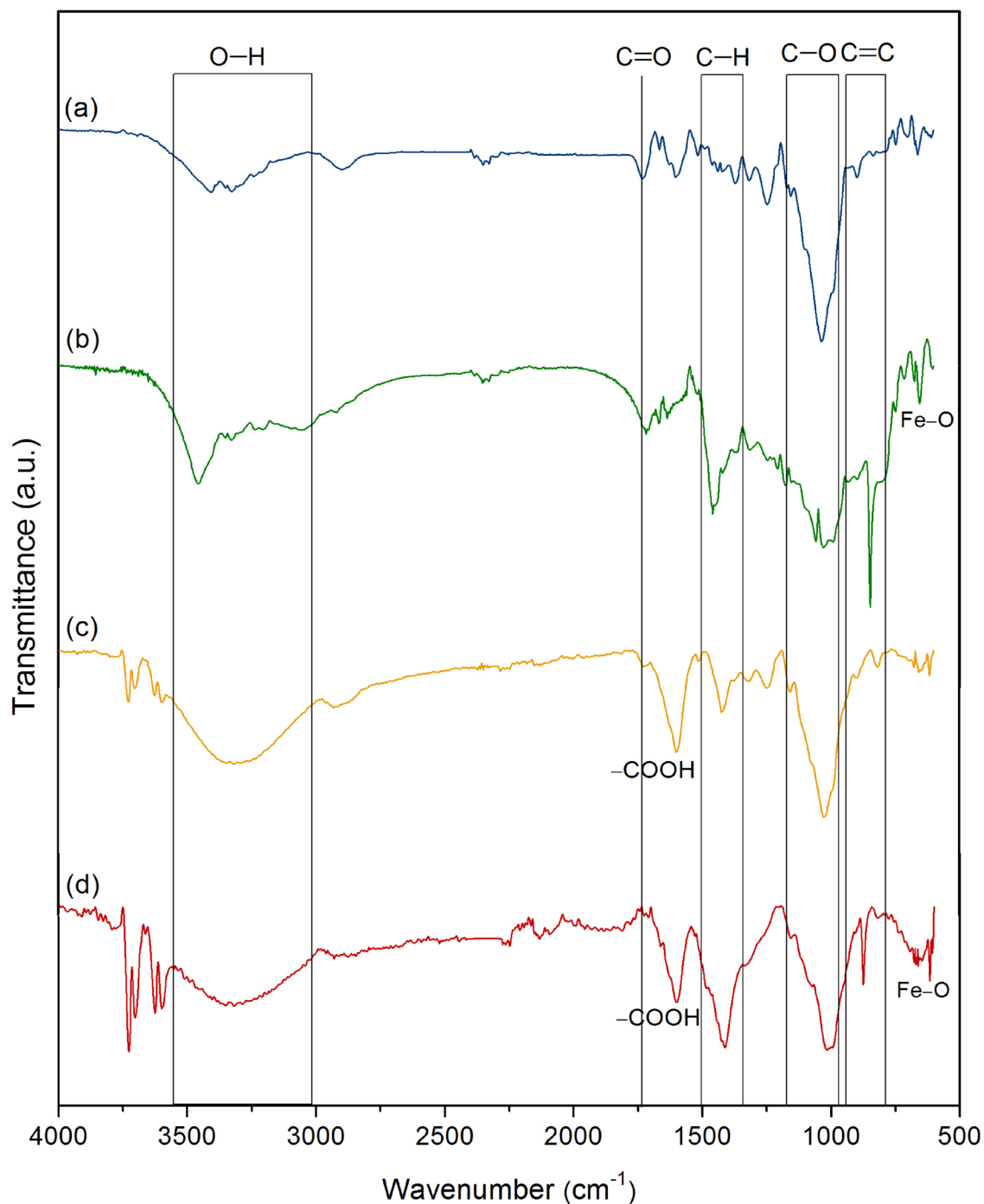


Figure 4. The chemical functional groups of (a) sugarcane bagasse powder (SB), (b) sugarcane bagasse powder doped iron(III) oxide-hydroxide (SBF), (c) sugarcane bagasse powder beads (SBB), and (d) sugarcane bagasse powder doped iron(III) oxide-hydroxide beads (SBFB) by FT-IR spectra analysis.

the increase of concentration because lead ions were more than the available active sites of bagasse adsorbent materials similar to the report by other studies^{9,33,37,38,45}. Lead removal efficiencies from 5 to 30 mg/L of SB, SBF, SBB, and SBFB were 40.63–100%, 92.78–100%, 78.07–100%, and 96.19–100%, respectively. For the lead concentration of 10 mg/L, lead removal efficiencies of SB, SBF, SBB, and SBFB were 96.08%, 100%, 98.22%, and 100%, respectively, and SBFB demonstrated the highest lead removal efficiency of other materials.

In conclusion, 0.6 g, 6 h, pH 5, 10 mg/L, 0.2 g, 3 h, pH 5, 10 mg/L, 0.2 g, 2 h, pH 5, 10 mg/L, and 0.1 g, 2 h, pH 5, 10 mg/L were the optimum conditions in dose, contact time, pH, and concentration of SB, SBF, SBB, and SBFB, respectively, and they could be arranged in order from high to low of SBFB > SBF > SBB > SB. As a result, the changing material form and adding iron(III) oxide-hydroxide helped to improve material efficiency for lead adsorption, and SBFB was recommended to be further applied for lead removal in the wastewater treatment system.

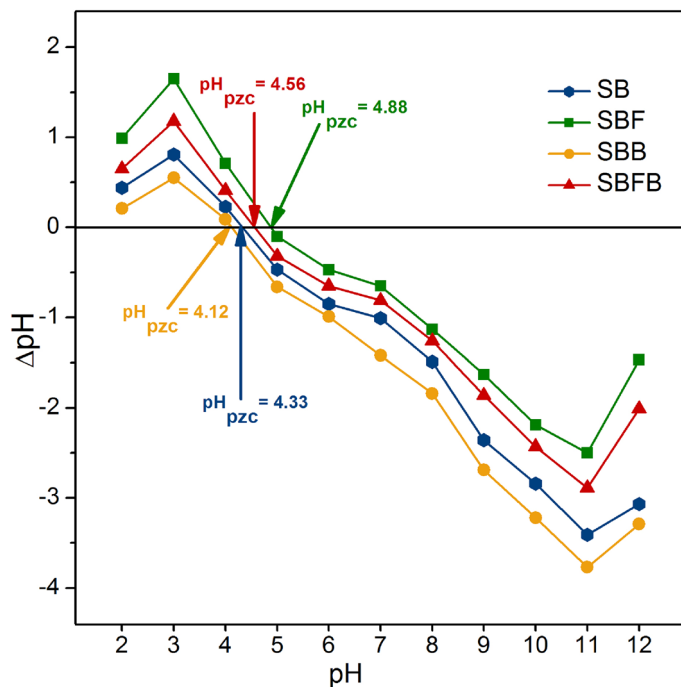


Figure 5. The point of zero charges of sugarcane bagasse powder (SB), sugarcane bagasse powder doped iron(III) oxide-hydroxide (SBF), sugarcane bagasse powder beads (SBB), and sugarcane bagasse powder doped iron(III) oxide-hydroxide beads (SBFB) for lead adsorptions.

Adsorption isotherms. The adsorption isotherm was designed to investigate the adsorption patterns of SB, SBF, SBB, and SBFB for lead adsorptions. Linear and nonlinear models of Langmuir, Freundlich, Temkin, and Dubinin–Radushkevich models were studied. For linear models, Langmuir, Freundlich, Temkin, and Dubinin–Radushkevich isotherms were plotted by C_e/q_e versus C_e , $\log q_e$ versus $\log C_e$, q_e versus $\ln C_e$, and $\ln q_e$ versus ε^2 , respectively. For nonlinear models, all isotherms were plotted by C_e versus q_e . The graph plotting results and the equilibrium isotherm parameters were demonstrated in Fig. 7a–e and Table 3, respectively.

For the linear Langmuir model, Langmuir maximum adsorption capacities (q_m) of SB, SBF, SBB, and SBFB were 6.161, 27.027, 23.697, and 57.471 mg/g, respectively, and Langmuir adsorption constants (K_L) of SB, SBF, SBB, and SBFB were 1.337, 5.362, 3.431, and 6.692 L/mg, respectively. For the nonlinear Langmuir model, Langmuir maximum adsorption capacities (q_m) of SB, SBF, SBB, and SBFB were 6.193, 28.027, 23.659, and 57.505 mg/g, respectively, and Langmuir adsorption constants (K_L) of SB, SBF, SBB, and SBFB were 1.357, 5.452, 3.420, and 6.651 L/mg, respectively. For the linear Freundlich isotherm, the $1/n$ values of SB, SBF, SBB, and SBFB were 0.104, 0.155, 0.125, and 0.164, respectively. Freundlich adsorption constants (K_f) of SB, SBF, SBB, and SBFB were 4.091, 20.160, 17.022, and 44.005 (mg/g) (L/mg) $^{1/n}$, respectively. For the nonlinear Freundlich isotherm, the $1/n$ values of SB, SBF, SBB, and SBFB were 0.105, 0.154, 0.127, and 0.167, respectively. Freundlich adsorption constants (K_f) of SB, SBF, SBB, and SBFB were 4.139, 20.165, 17.019, and 45.029 (mg/g) (L/mg) $^{1/n}$, respectively. For the linear Temkin isotherm, b_T values of SB, SBF, SBB, and SBFB were 7.457×10^3 , 1.295×10^3 , 1.629×10^3 , and 0.599×10^3 J/mol, respectively. A_T values of SB, SBF, SBB, and SBFB were 5.427×10^5 , 0.510×10^5 , 1.403×10^5 , and 0.429×10^5 L/g, respectively. For the nonlinear Temkin isotherm, b_T values of SB, SBF, SBB, and SBFB were 7.461×10^3 , 1.298×10^3 , 1.626×10^3 , and 0.609×10^3 J/mol, respectively. A_T values of SB, SBF, SBB, and SBFB were 5.467×10^5 , 0.516×10^5 , 1.415×10^5 , and 0.433×10^5 L/g, respectively. For the linear Dubinin–Radushkevich model, the maximum adsorption capacities (q_m) of SB, SBF, SBB, and SBFB were 4.648, 19.556, 19.184, and 40.419 mg/g, respectively, and the activity coefficient (K_{DR}) values of SB, SBF, SBB, and SBFB were 0.002, 0.003, 0.003, and 0.003 mol 2 /J 2 , respectively. The adsorption energy (E) values of SB, SBF, SBB, and SBFB were 15.811, 13.363, 12.500, and 13.363 kJ/mol, respectively. For the nonlinear Dubinin–Radushkevich model, the maximum adsorption capacities (q_m) of SB, SBF, SBB, and SBFB were 4.660, 19.560, 19.176, and 40.190 mg/g, respectively, and the activity coefficient (K_{DR}) values of SB, SBF, SBB, and SBFB were 0.002, 0.003, 0.005, and 0.004 mol 2 /J 2 , respectively. The adsorption energy (E) values of SB, SBF, SBB, and SBFB were 15.233, 12.467, 10.266, and 11.924 kJ/mol, respectively.

For the R^2 value consideration, the R^2 values of SB, SBF, SBB, and SBFB in the linear Langmuir model were 0.966, 0.944, 0.987, and 0.948, respectively, and their R^2 values in the linear Freundlich model were 0.930, 0.951, 0.861, and 0.951, respectively. For the linear Temkin model, the R^2 values of SB, SBF, SBB, and SBFB were 0.790, 0.813, 0.867, and 0.818, respectively, and their R^2 values in the linear Dubinin–Radushkevich were 0.769, 0.832, 0.838, and 0.843, respectively. In addition, the R^2 values of SB, SBF, SBB, and SBFB in the nonlinear Langmuir model were 0.968, 0.946, 0.985, and 0.951, respectively, and their R^2 values in the nonlinear Freundlich model were 0.931, 0.953, 0.866, and 0.955, respectively. For the nonlinear Temkin model, the R^2 values of SB, SBF, SBB,

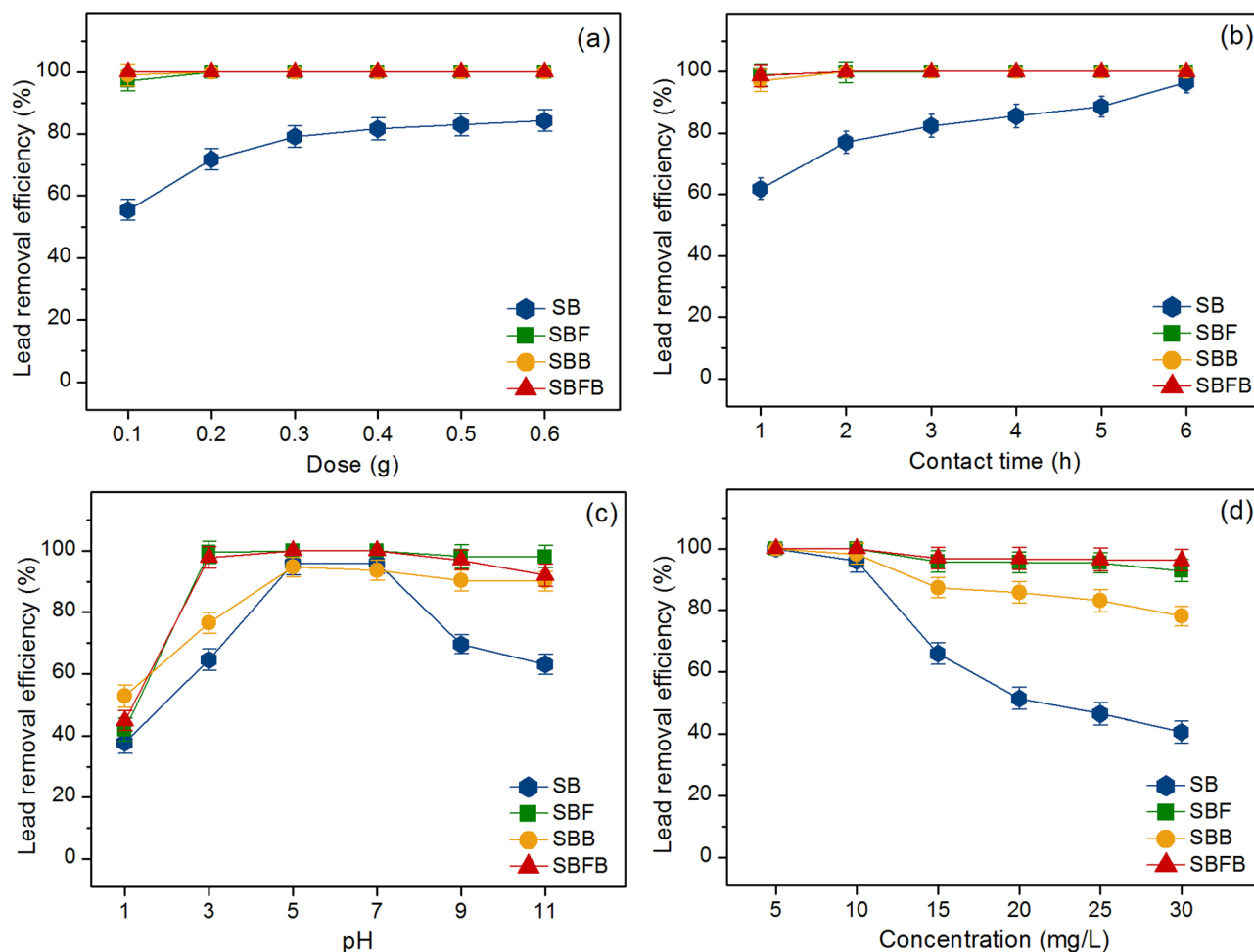


Figure 6. Batch experiments on the effects of (a) dose, (b) contact time, (c) pH, and (d) concentration of sugarcane bagasse powder (SB), sugarcane bagasse powder doped iron(III) oxide-hydroxide (SBF), sugarcane bagasse powder beads (SBB), and sugarcane bagasse powder doped iron(III) oxide-hydroxide beads (SBFB).

and SBFB were 0.791, 0.811, 0.865, and 0.819, respectively, and their R^2 values in the nonlinear Dubinin–Radushkevich were 0.768, 0.831, 0.831, and 0.845, respectively. Moreover, the R_{adj}^2 values of SB, SBF, SBB, and SBFB in the nonlinear Langmuir model were 0.960, 0.946, 0.982, and 0.950, respectively, and their R_{adj}^2 values in the nonlinear Freundlich model were 0.913, 0.952, 0.860, and 0.954, respectively. the R_{adj}^2 values of SB, SBF, SBB, and SBFB in the nonlinear Temkin model were 0.788, 0.810, 0.863, and 0.817, respectively, and their R_{adj}^2 values in nonlinear Dubinin–Radushkevich were 0.766, 0.829, 0.829, and 0.844.

Since the R^2 values of SB and SBB in both linear and nonlinear Langmuir models were higher than Freundlich, Temkin, and Dubinin–Radushkevich models, their adsorption patterns corresponded to Langmuir isotherm relating to a physical process with homogenous adsorption on adsorbent surfaces. Therefore, the maximum adsorption capacity (q_m) and Langmuir adsorption constant (K_L) were used for considering lead adsorption by SB and SBB. In Table 3, SBB demonstrated higher q_m and K_L values than SB, so SBB had higher lead adsorption with a faster reaction than SB. While the R^2 values of SBF and SBFB in both linear and nonlinear Freundlich models were higher than Langmuir, Temkin, and Dubinin–Radushkevich models, their adsorption patterns were Freundlich isotherm relating to a physiochemical process with heterogeneous adsorption on adsorbent surfaces. Therefore, the Freundlich adsorption constant (K_F) and a constant depiction of adsorption intensity ($1/n$) were used for explaining lead adsorption by SBF and SBFB. In Table 3, SBFB illustrated a higher K_F value than SBF, so SBFB might be faster lead adsorption than SBF. Since $1/n$ values of SBF and SBFB had less than 1 that meant both materials were favorable lead adsorptions. Moreover, both linear and nonlinear isotherm models were recommended to plot graphs for confirming the results and protecting against data mistranslation^{45,47–50}.

Moreover, the comparison of the maximum adsorption capacity (q_m) value of sugarcane bagasse adsorbent materials with and without modifications for lead adsorption in an aqueous solution is illustrated in Table 4. For unmodified comparison, SB had a higher q_m value than the study of Ezeonuegbu et al.⁹ while it had a closely q_m value to Matin-Lara et al.⁵¹ For modified comparison, the q_m values of SB, SBF, SBB, and SBFB had higher values than other studies except for the studies of modified sugarcane bagasse with acid, alkaline, or metal oxides with acid or alkaline modifications. In this study, SBFB presented the highest q_m value which meant that SBFB had possibly the highest lead adsorption property than other materials.

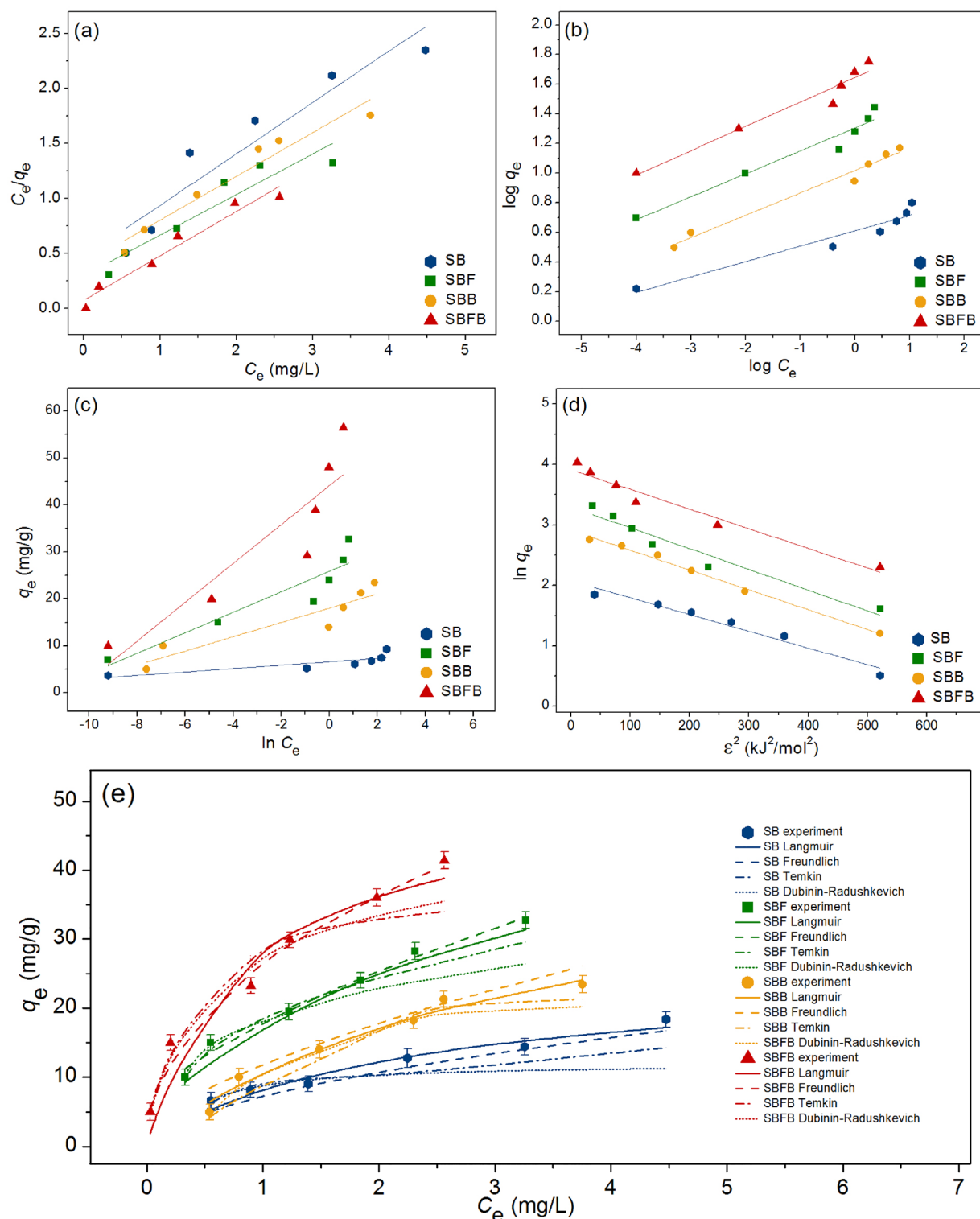


Figure 7. Graphs of (a) linear Langmuir, (b) linear Freundlich, (c) linear Temkin, (d) linear Dubinin–Radushkevich, and (e) nonlinear adsorption isotherms of sugarcane bagasse powder (SB), sugarcane bagasse powder doped iron(III) oxide-hydroxide (SBF), sugarcane bagasse powder beads (SBB), and sugarcane bagasse powder doped iron(III) oxide-hydroxide beads (SBFB) for lead adsorptions.

Adsorption kinetics. The adsorption kinetics are designed for understanding the adsorption mechanism and rate of reaction of lead adsorptions by SB, SBF, SBB, and SBFB. Various kinetic models of the pseudo-first-order kinetic, pseudo-second-order kinetic, elovich, and intraparticle diffusion models for plotting linear and

Regression methods	Isotherm models	Parameters	SB	SBF	SBB	SBFB
Linear	Langmuir	q_m (mg/g)	6.161	27.027	23.697	57.471
		K_L (L/mg)	1.337	5.362	3.431	6.692
		R^2	0.966	0.944	0.987	0.948
	Freundlich	$1/n$	0.104	0.155	0.125	0.164
		K_F (mg/g) (L/mg) ^{1/n}	4.091	20.160	17.022	44.005
		R^2	0.930	0.951	0.861	0.951
	Temkin	b_T ($\times 10^3$) (J/mol)	7.457	1.295	1.629	0.599
		A_T ($\times 10^5$) (L/g)	5.427	0.510	1.403	0.429
		R^2	0.790	0.813	0.867	0.818
	Dubinin–Radushkevich	q_m (mg/g)	4.648	19.556	19.184	40.419
		K_{DR} (mol ² /J ²)	0.002	0.003	0.003	0.003
		E (kJ/mol)	15.811	13.363	12.500	13.363
R^2		0.769	0.832	0.838	0.843	
Nonlinear	Langmuir	q_m (mg/g)	6.193	28.027	23.659	57.505
		K_L (L/mg)	1.357	5.452	3.420	6.651
		R^2	0.968	0.946	0.985	0.951
		R_{adj}^2	0.960	0.946	0.982	0.950
		RMSE	0.383	5.493	5.576	10.787
	Freundlich	$1/n$	0.105	0.154	0.127	0.167
		K_F (mg/g) (L/mg) ^{1/n}	4.139	20.165	17.019	45.029
		R^2	0.931	0.953	0.866	0.955
		R_{adj}^2	0.913	0.952	0.860	0.954
		RMSE	0.383	2.909	2.438	5.640
	Temkin	b_T ($\times 10^3$) (J/mol)	7.461	1.298	1.626	0.609
		A_T (L/g)	5.467	0.516	1.415	0.433
		R^2	0.791	0.811	0.865	0.819
		R_{adj}^2	0.788	0.810	0.863	0.817
		RMSE	0.850	4.099	2.874	8.310
	Dubinin–Radushkevich	q_m (mg/g)	4.660	19.560	19.176	41.190
		K_{DR} (mol ² /J ²)	0.002	0.003	0.005	0.004
		E (kJ/mol)	15.233	12.467	10.266	11.924
		R^2	0.768	0.831	0.831	0.845
		R_{adj}^2	0.766	0.829	0.829	0.844
RMSE	0.680	3.635	1.962	7.402		

Table 3. The comparison of linear and nonlinear isotherm parameters for lead adsorptions on sugarcane bagasse powder (SB), sugarcane bagasse powder doped iron(III) oxide-hydroxide (SBF), sugarcane bagasse powder beads (SBB), and sugarcane bagasse powder doped iron(III) oxide-hydroxide beads (SBFB).

nonlinear models were investigated. For linear models, they were plotted by $\ln(q_e - q_t)$ versus time (t), t/q_t versus time (t), q_t versus $\ln t$, and q_t versus time ($t^{0.5}$) for pseudo-first-order kinetic, pseudo-second-order kinetic, elovich, and intraparticle diffusion models, respectively. For nonlinear models, they were plotted by q_t versus time (t). The graph plotting results and the adsorption kinetic parameters were demonstrated in Fig. 8a–e and Table 5, respectively.

For the linear pseudo-first-order kinetic model, the adsorption capacities (q_e) of SB, SBF, SBB, and SBFB were 5.204, 13.722, 8.549, and 34.460 mg/g, and the reaction of rate constants (k_1) of SB, SBF, SBB, and SBFB were 0.014, 0.020, 0.010, and 0.025 min⁻¹. For the nonlinear pseudo-first-order kinetic model, the adsorption capacities (q_e) of SB, SBF, SBB, and SBFB were 5.616, 14.806, 8.915, and 34.595 mg/g, and the reaction of rate constants (k_1) of SB, SBF, SBB, and SBFB were 0.016, 0.025, 0.013, and 0.024 min⁻¹. For the linear pseudo-second-order kinetic model, the adsorption capacities (q_e) of SB, SBF, SBB, and SBFB were 3.934, 11.455, 10.965, and 21.053 mg/g, and the reaction of rate constants (k_2) of SB, SBF, SBB, and SBFB were 0.003, 0.002, 0.002, and 0.003 g/mg min. For the nonlinear pseudo-second-order kinetic model, the adsorption capacities (q_e) of SB, SBF, SBB, and SBFB were 3.946, 11.903, 11.300, and 21.471 mg/g, and the reaction of rate constants (k_2) of SB, SBF, SBB, and SBFB were 0.003, 0.001, 0.001, and 0.002 g/mg min. For the linear elovich model, the initial adsorption rates (α) of SB, SBF, SBB, and SBFB were 0.047, 3.334, 4.354, and 0.918 mg/g/min, and the extents of surface coverage (β) of SB, SBF, SBB, and SBFB were 1.510, 0.494, 0.529, and 0.289 g/mg. For the nonlinear elovich model, the initial adsorption rates (α) of SB, SBF, SBB, and SBFB were 0.052, 3.457, 4.785, and 0.987 mg/g/min, and the extents of surface coverage (β) of SB, SBF, SBB, and SBFB were 1.654, 0.565, 0.574, and 0.396 g/mg. For the linear intraparticle diffusion model, the reaction of rate constants (k_i) of SB, SBF, SBB, and SBFB were 0.146, 0.444,

Modifications	q_m (mg/g)	Refs
Unmodified	1.61	9
Unmodified	6.37	51
Biochar	12.74	10
Citric acid	52.63	52
Sulphuric acid	7.30	51
Nitric acid	18.72	14
Sodium hydroxide	21.24	14
Succinic anhydride	416.70	46
Succinic anhydride/alginat	354.60	34
Hydrothermal carbonization (HTC)/KOH activation	92.24	53
Fe ₃ O ₄ /citric acid	116.70	54
Fe ₃ O ₄ /co-precipitation	526.32	55
Fe ₃ O ₄ /formaldehyde	555.56	55
Fe ₃ O ₄ /NaOH and urea	666.67	55
Nano-hematite	16.57	42
ZnCl ₂ -activated carbon	19.30	12
Sugarcane bagasse powder (SB)	6.16	This study
Sugarcane bagasse powder doped iron(III) oxide-hydroxide (SBF)	27.03	This study
Sugarcane bagasse beads (SBB)	23.70	This study
Sugarcane bagasse powder doped iron(III) oxide-hydroxide beads (SBFB)	57.47	This study

Table 4. Comparison of the maximum adsorption capacity for lead adsorption of various sugarcane bagasse adsorbents.

0.430, and 0.704 mg/g min^{0.5}, and the constant C_i values of SB, SBF, SBB, and SBFB were 0.490, 2.276, 1.756, and 7.974 mg/g. For the nonlinear intraparticle diffusion model, the reaction of rate constants (k_i) of SB, SBF, SBB, and SBFB were 0.153, 0.451, 0.450, and 0.875 mg/g min^{0.5}, and the constant C_i values of SB, SBF, SBB, and SBFB were 0.510, 2.987, 1.815 and 8.013 mg/g.

For R^2 value consideration, the R^2 values of SB, SBF, SBB, and SBFB in the linear pseudo-first-order kinetic model were 0.911, 0.979, 0.975, and 0.968, and their R^2 values in the linear pseudo-second-order kinetic model were 0.991, 0.992, 0.992, and 0.998. In addition, the R^2 values of SB, SBF, SBB, and SBFB in the linear elovich model were 0.901, 0.912, 0.946, and 0.954, and their R^2 values in the linear intraparticle diffusion model were 0.867, 0.814, 0.906, and 0.730. In addition, the R^2 values of SB, SBF, SBB, and SBFB in the nonlinear pseudo-first-order kinetic model were 0.913, 0.977, 0.977, and 0.971, and their R^2 values in the nonlinear pseudo-second-order kinetic model were 0.993, 0.995, 0.996, and 0.996. Moreover, the R^2 values of SB, SBF, SBB, and SBFB in the nonlinear elovich model were 0.906, 0.915, 0.949, and 0.955, and their R^2 values in the nonlinear intraparticle diffusion model were 0.869, 0.816, 0.910, and 0.736. Moreover, the R_{adj}^2 values of SB, SBF, SBB, and SBFB in the nonlinear pseudo-first-order kinetic model were 0.910, 0.976, 0.976, and 0.970, and their R_{adj}^2 values in the nonlinear pseudo-second-order kinetic model were 0.992, 0.994, 0.996, and 0.996. In addition, the R_{adj}^2 values of SB, SBF, SBB, and SBFB in the nonlinear elovich model were 0.902, 0.911, 0.948, and 0.953, and their R_{adj}^2 values in the nonlinear intraparticle diffusion model were 0.864, 0.809, 0.907, and 0.727. Since the R^2 values of SB, SBF, SBB, and SBFB in both linear and nonlinear pseudo-second-order kinetic models were higher than pseudo-first-order kinetic, elovich, and intraparticle diffusion models, so their adsorption rate and mechanism of all sugarcane bagasse adsorbent materials corresponded to pseudo-second-order kinetic model with relating to a chemisorption process with heterogeneous adsorption with corresponding to the results of previous studies used sugarcane bagasse for removing lead, nickel, reactive blue 4 dye, and congo red^{19,39,40,56}. Therefore, the adsorption capacity (q_e) and the pseudo-second-order kinetic rate constant (k_2) were used for describing the rate and mechanism of all sugarcane adsorbent materials. In Table 5, SBFB had the highest q_e value than other materials, and it could be arranged from high to low of SBFB > SBF > SBB > SB. For k_2 , they had a close value to each other in a range of 0.001–0.003 g/mg min, so it had no significantly different in the kinetic rate constant for lead adsorption on all materials. Finally, the graph plotting of both linear and nonlinear kinetic models was also recommended for correct data translations^{40,41,49,50}.

Desorption experiments. The desorption experiments are designed to examine the reusability of sugarcane bagasse adsorbent materials for lead adsorptions to predict the investment budget and the feasibility of industrial applications from the economic view. Five adsorption–desorption cycles were applied for investigating the possible reusability of sugarcane bagasse adsorbent materials and their results are demonstrated in Fig. 9a–d. For SB, it could be reused in 5 cycles in ranges of adsorption at 73.11–96.15% and desorption at 66.02–94.07% with the decreasing of adsorption and desorption by 23% and 28%, respectively shown in Fig. 9a. In Fig. 9b, SBF could be reused in 5 cycles in ranges of adsorption at 83.92–100% and desorption at 75.12–97.24% with the decreasing of adsorption and desorption by 16% and 22%, respectively. For SBB, it could be reused in 5 cycles

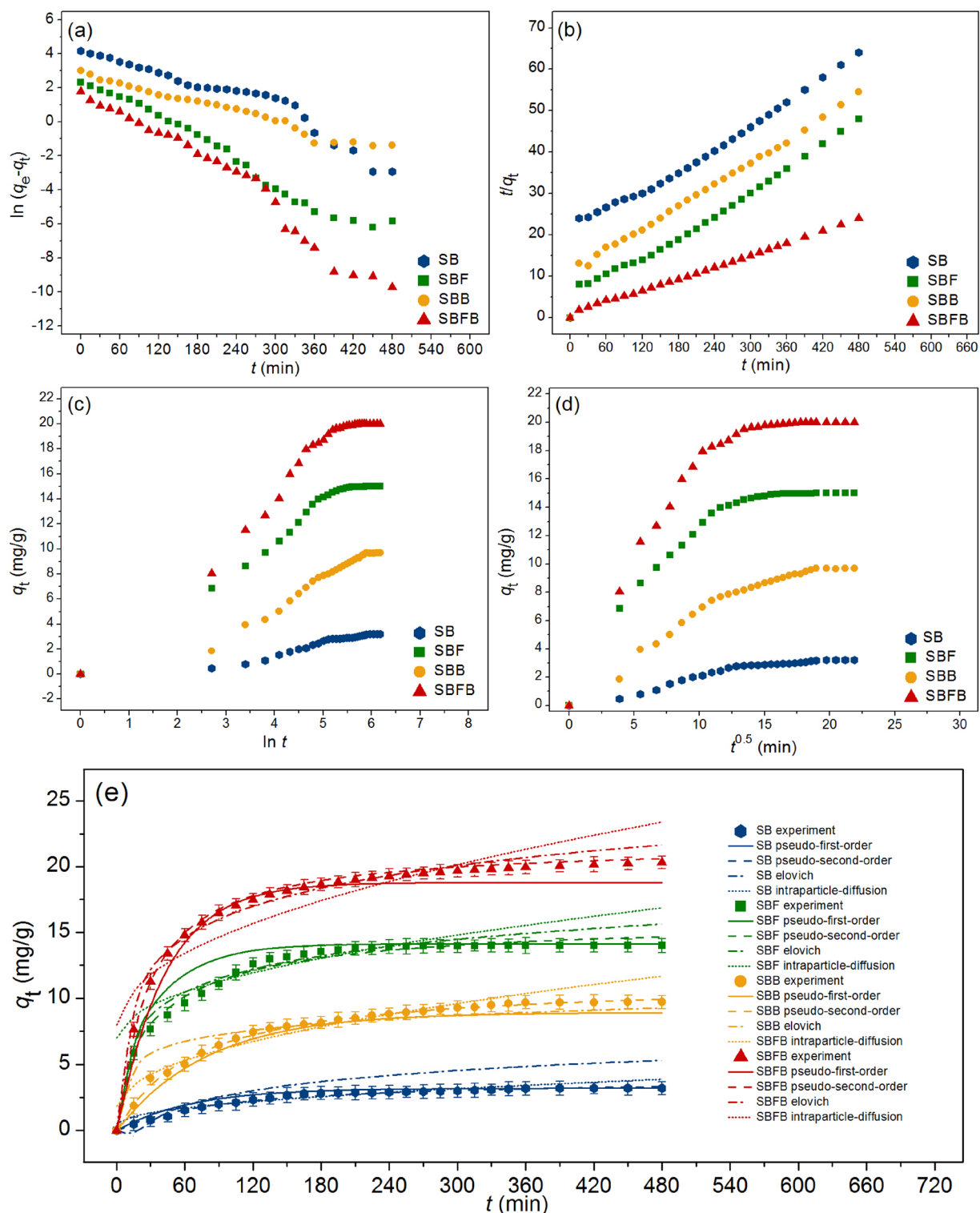


Figure 8. Graphs of (a) linear pseudo-first-order, (b) linear pseudo-second-order, (c) linear elovich model (d) linear intraparticle diffusion, and (e) nonlinear kinetic models of sugarcane bagasse powder (SB), sugarcane bagasse powder doped iron(III) oxide-hydroxide (SBF), sugarcane bagasse powder beads (SBB), and sugarcane bagasse powder doped iron(III) oxide-hydroxide beads (SBFB) for lead adsorptions.

in ranges of adsorption at 79.08–98.19% and desorption at 71.34–95.47% with the decreasing of adsorption and desorption by 19% and 24%, respectively illustrated in Fig. 9c. In Fig. 9d, SBFB could be reused in 5 cycles in ranges of adsorption at 87.96–100% and desorption at 81.27–98.37% with the decreasing of adsorption and

Regression methods	Kinetic models	Parameters	SB	SBF	SBB	SBFB
Linear	Pseudo-first-order kinetic	q_e (mg/g)	5.204	13.722	8.549	34.460
		k_1 (min^{-1})	0.014	0.020	0.010	0.025
		R^2	0.911	0.979	0.975	0.968
	Pseudo-second-order kinetic	q_e (mg/g)	3.934	11.455	10.965	21.053
		k_2 (g/mg min)	0.003	0.002	0.002	0.003
		R^2	0.991	0.992	0.992	0.998
	Elovich	α (mg/g/min)	0.047	3.334	4.354	0.918
		β (g/mg)	1.510	0.494	0.529	0.289
		R^2	0.901	0.912	0.946	0.954
	Intraparticle diffusion	k_i ($\text{mg/g min}^{0.5}$)	0.146	0.444	0.430	0.704
		C_i (mg/g)	0.490	2.276	1.756	7.974
		R^2	0.867	0.814	0.906	0.730
Nonlinear	Pseudo-first-order kinetic	q_e (mg/g)	5.616	14.806	8.915	34.595
		k_1 (min^{-1})	0.016	0.025	0.013	0.024
		R^2	0.913	0.977	0.977	0.971
		R_{adj}^2	0.910	0.976	0.976	0.970
		RMSE	0.267	1.016	0.576	1.120
	Pseudo-second-order kinetic	q_e (mg/g)	3.946	11.903	11.300	21.471
		k_2 (g/mg min)	0.003	0.001	0.001	0.002
		R^2	0.993	0.995	0.996	0.996
		R_{adj}^2	0.992	0.994	0.996	0.996
		RMSE	0.107	0.415	0.153	0.520
	Elovich	α (mg/g/min)	0.052	3.457	4.785	0.987
		β (g/mg)	1.654	0.565	0.574	0.396
		R^2	0.906	0.915	0.949	0.955
		R_{adj}^2	0.902	0.911	0.948	0.953
		RMSE	1.283	0.788	1.018	0.976
	Intraparticle diffusion	k_i ($\text{mg/g min}^{0.5}$)	0.153	0.451	0.450	0.875
		C_i (mg/g)	0.510	2.987	1.815	8.013
		R^2	0.869	0.816	0.910	0.736
		R_{adj}^2	0.864	0.809	0.907	0.727
		RMSE	0.603	2.666	1.564	4.391

Table 5. The comparison of linear and nonlinear kinetic parameters for lead adsorptions on sugarcane bagasse powder (SB), sugarcane bagasse powder doped iron(III) oxide-hydroxide (SBF), sugarcane bagasse powder beads (SBB), and sugarcane bagasse powder doped iron(III) oxide-hydroxide beads (SBFB).

desorption by 12% and 17%, respectively. Therefore, all sugarcane adsorption materials could be reused in more than 5 cycles for lead adsorptions, and they are potential materials for further industrial applications.

The application and environmental feasibility of materials. This study presented four new biosorbent materials from sugarcane bagasse including two material forms of powder and bead forms as choices of users for lead adsorption in wastewater. Four synthesized sugarcane adsorbent materials of SB, SBF, SBB, and SBFB demonstrated high lead adsorptions of more than 96%, so all materials are potential adsorbents for lead removal in an aqueous solution. However, the operation cost might be a significant point for user consideration in industrial applications. Since SBB and SBFB are bead materials, they are easier separate from treated wastewater than SB and SBF. Especially, SBFB is a good option than SBB because it spent less material dosage and contact time than SBB for 100% lead removal including it could be reused more than 5 cycles with a low adsorption capacity loss of approximately 13%. Moreover, sugarcane bagasse is a large amount of waste from sugar factories in Thailand. Therefore, if the sugarcane bagasse can be utilized by synthesizing biosorbent for lead removal, it may be another way to utilize waste for reducing waste management and help reduce lead contamination in the wastewater in another way as well. Therefore, SBFB might be a potential material for applying industrial applications for lead adsorption in the future.

The possible mechanism of lead adsorption by sugarcane bagasse adsorbent materials

The possible mechanism of lead adsorption on SB, SBF, SBB, and SBFB was explained in Fig. 10. The main structure of sugarcane bagasse adsorbent materials is composed of cellulose, hemicellulose, and lignin confirmed by detecting the specific cellulose peaks represented in XRD analysis. Moreover, the main chemical functional

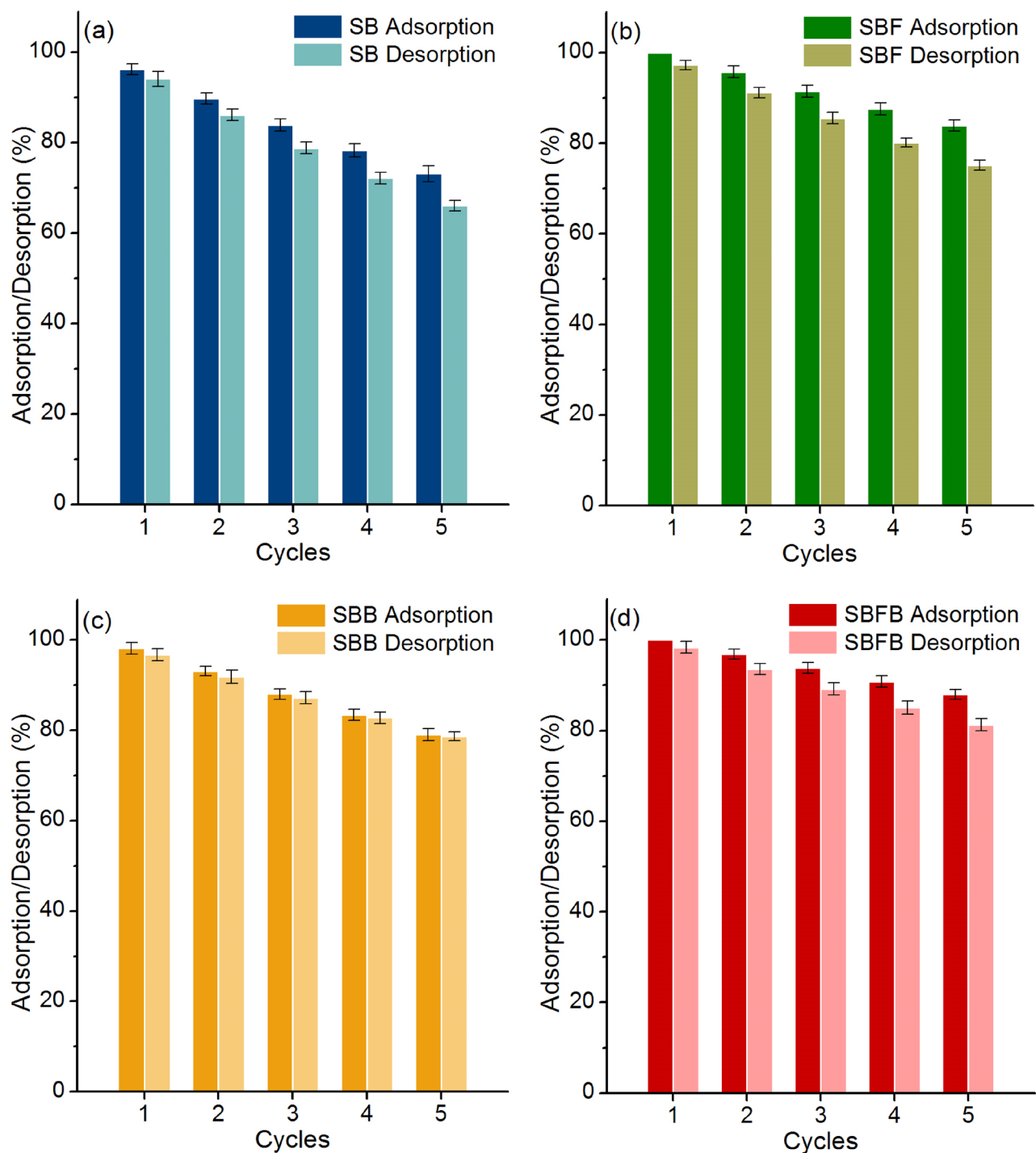


Figure 9. The desorption experiments of (a) sugarcane bagasse powder (SB), (b) sugarcane bagasse powder doped iron(III) oxide-hydroxide (SBF), (c) sugarcane bagasse powder beads (SBB), and (d) sugarcane bagasse powder doped iron(III) oxide-hydroxide beads (SBFB) for lead adsorptions.

groups of contained carboxyl groups ($-\text{COOH}$) or hydroxyl groups ($-\text{OH}$) were found in all materials by FT-IR analysis. When SB was added by iron(III) oxide-hydroxide to be SBF, they formed the complex compound of iron(III) oxide-hydroxide precipitation on the surface of SB in form of $\text{SB}\cdot\text{Fe}(\text{OH})_3$ by sharing electrons with hydroxyl groups of sugarcane bagasse. In addition, SBB formed the complex compound of SB and sodium alginate whose main structure had a carboxyl group ($-\text{COOH}$) similar to the main compounds of sugarcane bagasse materials. For SBFB, it formed a complex compound by adding iron(III) oxide-hydroxide and sodium alginate similar to SBF and SBB. The possible mechanism of lead adsorptions by sugarcane bagasse adsorbent materials might occur from donating a proton (H^+) from carboxyl groups ($-\text{COOH}$) or hydroxyl groups ($-\text{OH}$) or $\text{SB}\cdot\text{Fe}(\text{OH})_3$ of main chemical compounds or complex compounds to be $-\text{COO}^-$ or $-\text{O}^-$ or $\text{FeO}(\text{OH})_2$ for

capturing lead(II) ions (Pb^{2+}) by instead of H^+ from a process of electrostatic interaction⁵³. Especially, the pH of the solution ($\text{pH}_{\text{solution}}$) might affect how much lead is absorbed by the adsorbent. The previous studies found high lead adsorption in $\text{pH}_{\text{solution}} > \text{pH}_{\text{pzc}}$ and reported in a range of pH 4–6^{9,33,45} which corresponded to high lead removal efficiencies of all sugarcane adsorbent materials at pH 5 in this study from the batch experiments. Moreover, these results are supported by the results of pH_{pzc} of all materials at $\text{pH} > 4$.

Conclusion

This study successfully synthesized sugarcane bagasse powder (SB), sugarcane bagasse powder doped iron(III) oxide-hydroxide (SBF), sugarcane bagasse powder beads (SBB), and sugarcane bagasse powder doped iron(III) oxide-hydroxide beads (SBFB). The crystalline patterns of all sugarcane bagasse adsorbent materials were amorphous phases presenting specific peaks of cellulose. The sodium alginate peaks were detected in SBB and SBFB whereas iron(III) oxide-hydroxide peaks were only found in SBF and SBFB. The surface morphologies of SB and SBF were scales or overlapping plate surfaces whereas SBB and SBFB had spherical shapes with coarse surfaces. The main chemical compositions of all sugarcane bagasse adsorbent materials were C, O, and Ca, and Na and Cl were detected in all materials except SB. Fe was only found in SBF and SBFB because of adding iron(III) oxide-hydroxide to raw materials. Five main chemical functional groups of all materials were O–H, C=O, C–H, C–O, and C=C, whereas Fe–O and –COOH were only found in materials with adding iron(III) oxide-hydroxide or bead material. The pH_{pzc} of SB, SBF, SBB, and SBFB were 4.33, 4.88, 4.12, and 4.56, respectively. For batch experiments, the optimum conditions of SB, SBF, SBB, and SBFB were 0.6 g, 6 h, pH 5, 10 mg/L, 0.2 g, 3 h, pH 5, 10 mg/L, 0.2 g, 2 h, pH 5, 10 mg/L, and 0.1 g, 2 h, pH 5, 10 mg/L, respectively. Lead removal efficiencies of SB, SBF, SBB, and SBFB of 10 mg/L were 96.08%, 100%, 98.22%, and 100%, respectively, and it could be arranged in order from high to low of SBFB > SBF > SBB > SB. Thus, adding iron(III) oxide-hydroxide and changing material form helped to improve material efficiencies for lead adsorptions. For adsorption isotherms, SB and SBB corresponded to the Langmuir model related to a physical adsorption process whereas SBF and SBFB corresponded to the Freundlich model correlated to a physicochemical adsorption process. For the kinetic study, they corresponded to a pseudo-second-order kinetic model related to a chemisorption process with heterogeneous adsorption. All materials could be reused for more than 5 cycles with a lead removal efficiency of more than 73%. Therefore, all sugarcane bagasse adsorbent materials were high potential materials for lead adsorptions in an aqueous solution, and SBFB demonstrated the highest lead removal efficiency. Therefore, SBFB was a suitable material to further apply to the wastewater treatment system of industry.

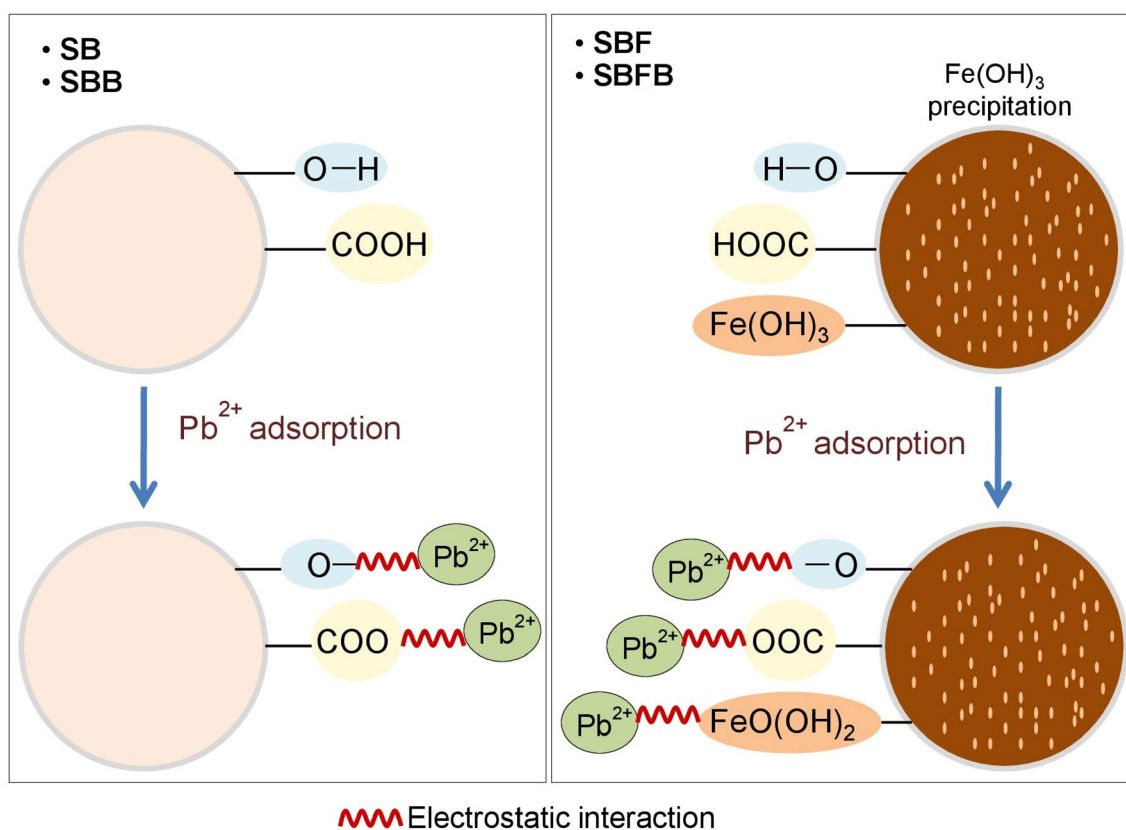


Figure 10. Possible mechanism of lead adsorption on sugarcane bagasse powder (SB), sugarcane bagasse powder doped iron(III) oxide-hydroxide (SBF), sugarcane bagasse powder beads (SBB), and sugarcane bagasse powder doped iron(III) oxide-hydroxide beads (SBFB).

For future works, the real wastewater with contaminated lead should be investigated to confirm the ability of sugarcane bagasse materials, and the continuous flow study also needs to study for further industrial applications.

Materials and methods

Raw material. Sugarcane bagasse was obtained from a local market in Khon Kaen province, Thailand.

Chemicals. All chemicals were analytical grades (AR) without purification before use. For modified bead materials, ferric chloride hexahydrate ($\text{FeCl}_3 \cdot 6\text{H}_2\text{O}$) (LOBA, India), sodium hydroxide (NaOH) (RCI Labscan, Thailand), sodium alginate ($\text{NaC}_6\text{H}_7\text{O}_6$) (Merck, Germany), and calcium chloride (CaCl_2) (Kemaus, New Zealand) were used. Lead nitrate ($\text{Pb}(\text{NO}_3)_2$) (QRëC, New Zealand) was used for preparing of wastewater sample. For the point of zero charge (pH_{pzc}) experiment, 0.1 M hydrochloric acid (HCl) (RCI Labscan, Thailand), 0.1 M NaOH and 0.1 M sodium chloride (NaCl) (RCI Labscan, Thailand) solutions were used. For the desorption experiments, a 0.5 M nitric acid (HNO_3) (Merck, Germany) solution was used. For pH adjustments, 1% HNO_3 and 1% NaOH solutions were used.

Synthesis of four adsorbent materials. The synthesis of four adsorbent materials which were sugarcane bagasse powder (SB), sugarcane bagasse powder doped iron(III) oxide-hydroxide (SBF), sugarcane bagasse powder beads (SBB), and sugarcane bagasse powder doped iron(III) oxide-hydroxide beads (SBFB) were demonstrated in Fig. 11, and the details were clearly explained below:

The synthesis of SB. Sugarcane bagasse was washed with tap water to remove contaminants, and then it was dried overnight in a hot air oven (Binder, FED 53, Germany) at 105 °C. It was ground and sieved in size of 125 μm and kept in a desiccator before use called sugarcane bagasse powder (SB).

The synthesis of SBF. SB of 5 g was added to 500 mL of Erlenmeyer flask containing 160 mL of 5% $\text{FeCl}_3 \cdot 6\text{H}_2\text{O}$, and it was mixed by an orbital shaker (GFL, 3020, Germany) of 200 rpm for 3 h. Then, it was filtrated and air-dried at room temperature for 12 h. After that, it was added to 500 mL of Erlenmeyer flask containing 160 mL of 5% NaOH, and it was mixed by an orbital shaker of 200 rpm for 1 h. Then, it was filtered, air-dried at room temperature for 12 h, and kept in a desiccator before use called sugarcane bagasse powder doped iron(III) oxide-hydroxide (SBF).

The synthesis of SBB or SBFB. SB or SBF of 5 g was added to 500 mL of beaker containing 200 mL of 2% sodium alginate, and then it was homogeneously mixed and heated by a hot plate (Ingenieurbüro CAT, M. Zipperer GmbH, M 6, Germany) at 60 °C with a constant stirring of 200 rpm. Then, it was dropped by drop by using a 10 mL syringe with a needle size of 1.2×40 mm into 250 mL of 0.1 M CaCl_2 . The beaded samples were soaked in 0.1 M CaCl_2 for 24 h, and then these were filtered and rinsed with DI water. After that, these were air-dried at room temperature for 12 h and kept in a desiccator before use called sugarcane bagasse powder beads (SBB) or sugarcane bagasse doped iron(III) oxide-hydroxide beads (SBFB).

Characterizations of sugarcane bagasse adsorbent materials. The crystalline structures, surface morphologies, chemical compositions, and chemical functional groups of SB, SBF, SBB, and SBFB were investigated by X-Ray Diffractometer (XRD) (PANalytical, EMPYREAN, United Kingdom) in the range of $2\theta = 5^\circ$ – 60° , Field Emission Scanning Electron Microscopy and Focus Ion Beam (FESEM-FIB) with Energy Dispersive X-Ray Spectrometer (EDX) (FEI, Helios NanoLab G3 CX, USA, and Fourier Transform Infrared Spectroscopy (FT-IR) (Bruker, TENSOR27, Hong Kong), respectively.

The point of zero charges of sugarcane bagasse adsorbent materials. The experiment of the point of zero charges of SB, SBF, SBB, and SBFB for lead adsorptions is applied from the study of Praipipat et al.⁴¹. The sample solutions of 0.1 M NaCl at pH values from 2 to 12 were prepared, and 0.1 M HCl and 0.1 M NaOH solutions were used for pH adjustments. Next, the material of 0.1 g was added to a 250 mL Erlenmeyer flask containing each sample solution of 50 mL, and it was shaken by an orbital shaker (GFL, 3020, Germany) at room temperature at 150 rpm for 24 h. After that, a final pH value was measured by (Mettler Toledo, SevenGo with InLab 413/IP67, Switzerland). Then, the ΔpH ($\text{pH}_{\text{final}} - \text{pH}_{\text{initial}}$) was calculated, and the point of zero charge (pH_{pzc}) was determined from a value point of the cross line of ΔpH versus $\text{pH}_{\text{initial}}$ equal to zero.

Batch adsorption experiments. A series of batch adsorption experiments were designed to investigate the effect of dose, contact time, pH, and concentration on lead removal efficiency by SB, SBF, SBB, and SBFB. The difference of dose from 0.1 to 0.6 g, contact time from 1 to 6 h, pH values of 1, 3, 5, 7, 9, 11, and lead concentration from 5 to 30 mg/L with the control condition of initial lead concentration of 10 mg/L, a sample volume of 200 mL, a shaking speed of 200 rpm, a temperature of 25 °C were applied. The lowest value of each affecting factor with the highest lead removal efficiency was selected as the optimum value, and that value was applied to the next affecting factor study. Lead concentrations were analyzed by an atomic adsorption spectrophotometer (PerkinElmer, PinAAcle 900 F, USA), and triplicate experiments were conducted to confirm the results. Lead removal in the percentage (%) is calculated by following Eq. (1).

$$\text{Lead removal efficiency (\%)} = (C_0 - C_e) / C_0 \times 100 \quad (1)$$

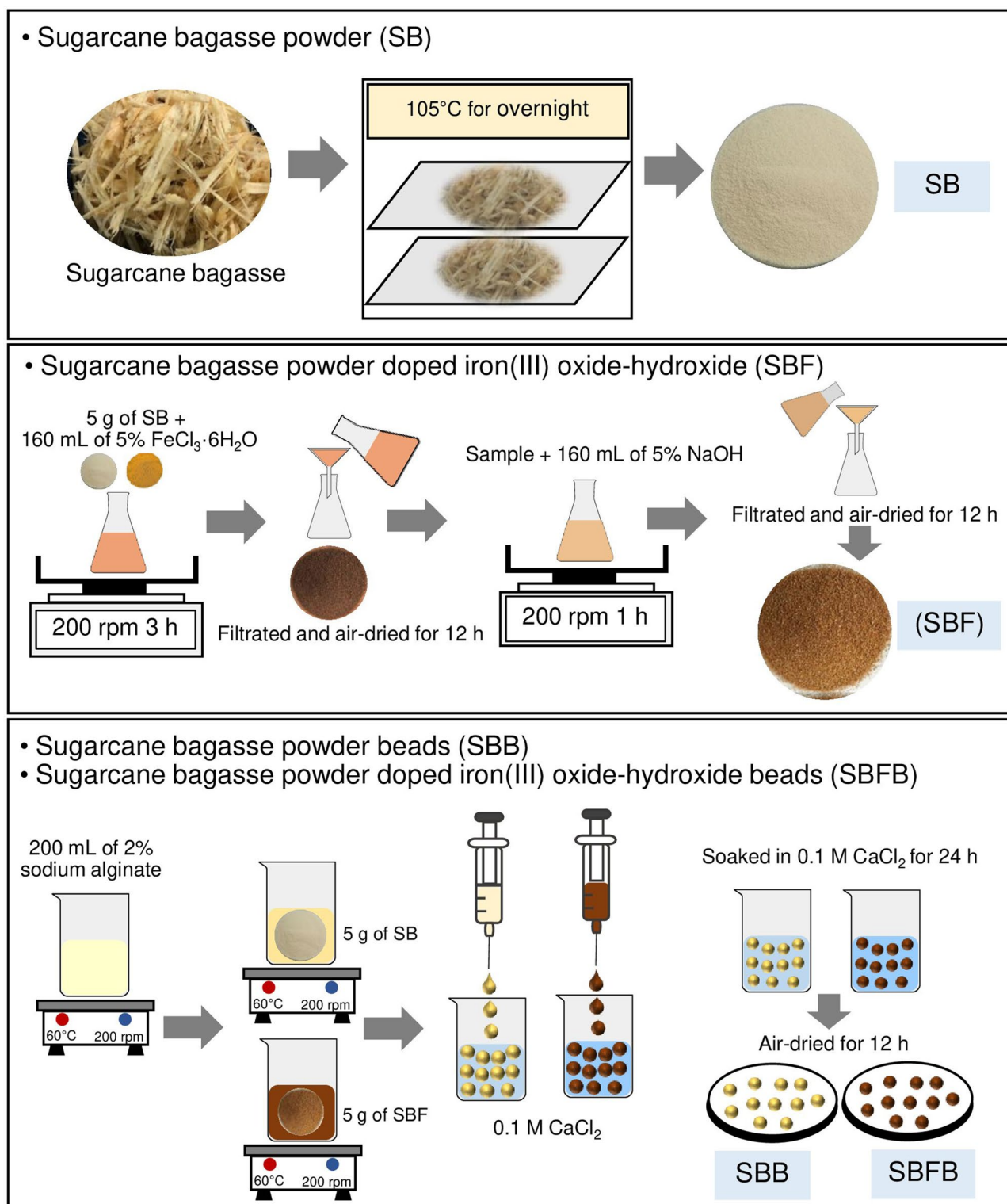


Figure 11. Flow diagrams of synthesis methods of sugarcane bagasse powder (SB), sugarcane bagasse powder doped iron(III) oxide-hydroxide (SBF), sugarcane bagasse powder beads (SBB), and sugarcane bagasse powder doped iron(III) oxide-hydroxide beads (SBFB).

where C_0 is the initial lead concentration (mg/L), and C_e is the equilibrium of lead concentration in the solution (mg/L).

Adsorption isotherms. Adsorption isotherms are designed to identify the adsorption pattern of adsorbent material which may be explained by the adsorption process of monolayer or multi-layer or heat or thermodynamic. Linear and nonlinear Langmuir, Freundlich, Temkin, and Dubinin–Radushkevich models are used to analyze followed Eqs. (2)–(9)^{57–60}.

Langmuir isotherm:

$$\text{Linear: } C_e/q_e = 1/q_m K_L + C_e/q_m \quad (2)$$

$$\text{Nonlinear: } q_e = q_m K_L C_e / (1 + K_L C_e) \quad (3)$$

Freundlich isotherm:

$$\text{Linear: } \log q_e = \log K_F + 1/n \log C_e \quad (4)$$

$$\text{Nonlinear: } q_e = K_F C_e^{1/n} \quad (5)$$

Temkin isotherm:

$$\text{Linear: } q_e = RT/b_T \ln A_T + RT/b_T \ln C_e \quad (6)$$

$$\text{Nonlinear: } q_e = RT/b_T \ln A_T C_e \quad (7)$$

Dubinin–Radushkevich isotherm:

$$\text{Linear: } \ln q_e = \ln q_m - K_{DR} \varepsilon^2 \quad (8)$$

$$\text{Nonlinear : } q_e = q_m \exp(-K_{DR} \varepsilon^2) \quad (9)$$

where C_e is the equilibrium of lead concentration (mg/L), q_e is the amount of adsorbed lead on adsorbent materials (mg/g), q_m is indicated the maximum amount of lead adsorption on adsorbent materials (mg/g), K_L is the adsorption constant (L/mg). K_F is the constant of adsorption capacity (mg/g) (L/mg)^{1/n}, and $1/n$ is the constant depicting the adsorption intensity⁶¹. R is the universal gas constant (8.314 J/mol K), T is the absolute temperature (K), b_T is the constant related to the heat of adsorption (J/mol), and A_T is the equilibrium binding constant corresponding to the maximum binding energy (L/g). q_m is the theoretical saturation adsorption capacity (mg/g), K_{DR} is the activity coefficient related to mean adsorption energy (mol²/J²), and ε is the Polanyi potential (J/mol). Graphs of linear Langmuir, Freundlich, Temkin, and Dubinin–Radushkevich isotherms were plotted by C_e/q_e versus C_e , $\log q_e$ versus $\log C_e$, q_e versus $\ln C_e$, and $\ln q_e$ versus ε^2 , respectively whereas graphs of their nonlinear were plotted by q_e versus C_e .

For adsorption isotherm experiments, 0.6 g of SB or 0.2 g of SBF or 0.2 g of SBB, or 0.1 g of SBFB were added to 500 mL Erlenmeyer flask with variable lead concentrations from 5 to 30 mg/L. The control condition of SB, SBF, SBB, and SBFB was a sample volume of 200 mL, a shaking speed of 200 rpm, pH 5, a temperature of 25 °C, and a contact time of 6 h for SB, 3 h for SBB, and 2 h for SBF and SBFB.

Adsorption kinetics. Adsorption kinetics are studied to investigate the adsorption mechanism of adsorbent material, and linear and nonlinear pseudo-first-order kinetic, pseudo-second-order kinetic, elovich, and intraparticle diffusion models were used following Eqs. (10)–(16)^{62–65}.

Pseudo-first-order kinetic model:

$$\text{Linear : } \ln(q_e - q_t) = \ln q_e - k_1 t \quad (10)$$

$$\text{Nonlinear: } q_t = q_e (1 - e^{-k_1 t}) \quad (11)$$

Pseudo-second-order kinetic model:

$$\text{Linear : } t/q_t = 1/k_2 q_e^2 + (t/q_e) \quad (12)$$

$$\text{Nonlinear: } q_t = k_2 q_e^2 t / (1 + q_e k_2 t) \quad (13)$$

Elovich model:

$$\text{Linear : } q_t = 1/\beta \ln \alpha \beta + 1/\beta \ln t \quad (14)$$

$$\text{Nonlinear : } q_t = \beta \ln t + \beta \ln \alpha \quad (15)$$

Intraparticle diffusion model:

$$\text{Linear and nonlinear: } q_t = k_1 t^{0.5} + C_i \quad (16)$$

where q_e is the amount of adsorbed lead on adsorbent materials (mg/g), q_t is the amount of adsorbed lead at the time (t) (mg/g), k_1 is a pseudo-first-order rate constant (min^{-1}), and k_2 is a pseudo-second-order rate constant ($\text{g/mg min}^{0.5}$). α is the initial adsorption rate (mg/g/min) and β is the extent of surface coverage (g/mg). k_i is the intraparticle diffusion rate constant ($\text{mg/g min}^{0.5}$) and C_i is the constant that gives an idea about the thickness of the boundary layer (mg/g). Graphs of linear pseudo-first-order, pseudo-second-order, elovich, and intraparticle diffusion models were plotted by $\ln(q_e - q_t)$ versus time (t), t/q_t versus time (t), q_t versus $\ln t$, and q_t versus time ($t^{0.5}$), respectively whereas their nonlinear graphs were plotted by the capacity of lead adsorbed by adsorbent materials at the time (q_t) versus time (t).

For adsorption kinetic experiments, 3 g of SB or 1 g of SBF or 1 g of SBB, or 0.5 g of SBFB were added to 1000 mL of breaker with a lead concentration of 10 mg/L. The control condition of SB, SBF, SBB, and SBFB was a sample volume of 1000 mL, a shaking speed of 200 rpm, pH 5, a temperature of 25 °C, and a contact time of 8 h.

Desorption experiments. The possible material reusability is a significant point for considering further industrial applications, so five adsorption–desorption cycles are used for investigating the abilities of SB, SBF, SBB, and SBFB for lead adsorptions through the desorption experiments. The saturated material of SB or SBF or SBB, or SBFB after the adsorption process was added to 500 mL of Erlenmeyer flask containing 200 mL of 0.5 M HNO_3 solution, and it was shaken by an incubator shaker (New Brunswick, Innova 42, USA) at 200 rpm for 6 h. After that, it was washed with deionization water and dried at room temperature, and then it is ready for the next adsorption cycle. Equation (17) is used for calculating the desorption efficiency in percentage.

$$\text{Desorption (\%)} = (q_d/q_a) \times 100 \quad (17)$$

where q_d is the amount of lead desorbed (mg/mL) and q_a is the amount of lead adsorbed (mg/mL).

Data availability

The datasets used and/or analyzed during the current study are available from the corresponding author upon reasonable request.

Received: 4 October 2022; Accepted: 23 January 2023

Published online: 26 January 2023

References

- Obeng-Gyasi, E. Sources of lead exposure in various countries. *Rev. Environ. Health* **34**, 25–34 (2019).
- Balali-Mood, M., Naseri, K., Tahergorabi, Z., Khazdair, M. R. & Sadeghi, M. Toxic mechanisms of five heavy metals: Mercury, lead, chromium, cadmium, and arsenic. *Front. Pharmacol.* **12**, 643972 (2021).
- Qasem, N. A. A., Mohammed, R. H. & Lawal, D. U. Removal of heavy metal ions from wastewater: A comprehensive and critical review. *Npj Clean Water* **4**, 1–15 (2021).
- Rashid, R., Shafiq, I., Akhter, P., Iqbal, M. J. & Hussain, M. A state-of-the-art review on wastewater treatment techniques: The effectiveness of adsorption method. *Environ. Sci. Pollut. Res.* **28**, 9050–9066 (2021).
- Ogunlalu, O., Oyekunle, I. P., Iwuozor, K. O., Aderibigbe, A. D. & Emenike, E. C. Trends in the mitigation of heavy metal ions from aqueous solutions using unmodified and chemically-modified agricultural waste adsorbents. *Curr. Res. Green Sustain. Chem.* **4**, 100188 (2021).
- Oladoye, P. O. Natural, low-cost adsorbents for toxic Pb(II) ion sequestration from (waste)water: A state-of-the-art review. *Chemosphere* **287**, 132130 (2022).
- Lee, S., Lingamdinne, L. P., Yang, J. K., Chang, Y. Y. & Koduru, J. R. Potential electromagnetic column treatment of heavy metal contaminated water using porous Gd_2O_3 -doped graphene oxide nanocomposite: Characterization and surface interaction mechanisms. *J. Water Process. Eng.* **41**, 102083 (2021).
- Lingamdinne, L. P., Koduru, J. R., Chang, Y. Y. & Karri, R. R. Process optimization and adsorption modeling of Pb(II) on nickel ferrite-reduced graphene oxide nano-composite. *J. Mol. Liq.* **250**, 202–211 (2018).
- Ezeonuegbu, B. A. *et al.* Agricultural waste of sugarcane bagasse as efficient adsorbent for lead and nickel removal from untreated wastewater: Biosorption, equilibrium isotherms, kinetics and desorption studies. *Biotechnol. Rep.* **30**, e00614 (2021).
- Poonam, Bharti, S. K. & Kumar, N. Kinetic study of lead (Pb^{2+}) removal from battery manufacturing wastewater using bagasse biochar as biosorbent. *Appl. Water Sci.* **8**, 1–13 (2018).
- El Nemr, A. *et al.* Utilization of sugarcane bagasse/ ZnCl_2 for sustainable production of microporous nano-activated carbons of type I for toxic Cr(VI) removal from aqueous environment. *Biomass Convers. Biorefinery* <https://doi.org/10.1007/s13399-021-01445-6> (2021).
- Van Tran, T., Bui, Q. T. P., Nguyen, T. D., Le, N. T. H. & Bach, L. G. A comparative study on the removal efficiency of metal ions (Cu^{2+} , Ni^{2+} , and Pb^{2+}) using sugarcane bagasse-derived ZnCl_2 -activated carbon by the response surface methodology. *Adsorpt. Sci. Technol.* **35**, 72–85 (2017).
- Cholico-González, D., Ortiz Lara, N., Fernández Macedo, A. M. & Chavez Salas, J. Adsorption behavior of Pb(II), Cd(II), and Zn(II) onto agave bagasse, characterization, and mechanism. *ACS Omega* **5**, 3302–3314 (2020).
- Mahmood-ul-Hassan, M., Suthar, V., Rafique, E., Ahmad, R. & Yasin, M. Kinetics of cadmium, chromium, and lead sorption onto chemically modified sugarcane bagasse and wheat straw. *Environ. Monit. Assess.* **187**, 1–11 (2015).
- Zhang, Y., Yue, X., Xu, W., Zhang, H. & Li, F. Amino modification of rice straw-derived biochar for enhancing its cadmium(II) ions adsorption from water. *J. Hazard. Mater.* **379**, 120783 (2019).
- Asim, N. *et al.* Development of effective and sustainable adsorbent biomaterial from an agricultural waste material: Cu(II) removal. *Mater. Chem. Phys.* **249**, 123128 (2020).
- Tolkou, A. K. *et al.* Chromium(VI) removal from water by lanthanum hybrid modified activated carbon produced from coconut shells. *Nanomaterials* **12**, 1067 (2022).
- Chen, M., Wang, X. & Zhang, H. Comparative research on selective adsorption of Pb(II) by biosorbents prepared by two kinds of modifying waste biomass: Highly-efficient performance, application and mechanism. *J. Environ. Manag.* **288**, 112388 (2021).

19. Kamal, K. H., Attia, M. S., Ammar, N. S. & Abou-Taleb, E. M. Kinetics and isotherms of lead ions removal from wastewater using modified corncob nanocomposite. *Inorg. Chem. Commun.* **130**, 108742 (2021).
20. Lin, G. *et al.* Selective removal behavior and mechanism of trace Hg(II) using modified corn husk leaves. *Chemosphere* **225**, 65–72 (2019).
21. Cai, W. *et al.* Preparation of amino-functionalized magnetic biochar with excellent adsorption performance for Cr(VI) by a mild one-step hydrothermal method from peanut hull. *Colloids Surf. A Physicochem. Eng. Asp.* **563**, 102–111 (2019).
22. Guo, J., Liu, X., Han, M., Liu, Y. & Ji, S. Poly(*N*-acryloyl-L-histidine)-modified wood sawdust as an efficient adsorbent for low-level heavy metal ions. *Cellulose* **27**, 8155–8167 (2020).
23. Kayalvizhi, K. *et al.* Adsorption of copper and nickel by using sawdust chitosan nanocomposite beads—A kinetic and thermodynamic study. *Environ. Res.* **203**, 111814 (2022).
24. Wijewardana, P. *et al.* Removal of Cu, Pb and Zn from stormwater using an industrially manufactured sawdust and paddy husk derived biochar. *Environ. Technol. Innov.* **28**, 102640 (2022).
25. Pillai, P., Kakadiya, N., Timaniya, Z., Dharaskar, S. & Sillanpaa, M. Removal of arsenic using iron oxide amended with rice husk nanoparticles from aqueous solution. *Mater. Today Proc.* **28**, 830–835 (2020).
26. Li, A. *et al.* Removal of heavy metals from wastewaters with biochar pyrolyzed from MgAl-layered double hydroxide-coated rice husk: Mechanism and application. *Bioresour. Technol.* **347**, 126425 (2022).
27. Zheng, L., Peng, D. & Meng, P. Corn-cob-supported aluminium-manganese binary oxide composite enhanced removal of cadmium ions. *Colloids Surf. A Physicochem. Eng. Asp.* **561**, 109–119 (2019).
28. Gran, S. *et al.* Development of cerium oxide/corn-cob nanocomposite: A cost-effective and eco-friendly adsorbent for the removal of heavy metals. *Polymers (Basel)* **13**, 4464 (2021).
29. Herrera-Barros, A., Tejada-Tovar, C., Villabona-Ortiz, A., González-Delgado, A. D. & Benitez-Monroy, J. Cd(II) and Ni(II) uptake by novel biosorbent prepared from oil palm residual biomass and Al₂O₃ nanoparticles. *Sustain. Chem. Pharm.* **15**, 100216 (2020).
30. Jin, X. *et al.* Functionalized porous nanoscale Fe₃O₄ particles supported biochar from peanut shell for Pb(II) ions removal from landscape wastewater. *Environ. Sci. Pollut. Res.* **29**, 37159–37169 (2022).
31. Sahu, N., Singh, J. & Koduru, J. R. Removal of arsenic from aqueous solution by novel iron and iron-zirconium modified activated carbon derived from chemical carbonization of *Tectona grandis* sawdust: Isotherm, kinetic, thermodynamic and breakthrough curve modelling. *Environ. Res.* **200**, 111431 (2021).
32. Lingamdinne, L. P., Yang, J. K., Chang, Y. Y. & Koduru, J. R. Low-cost magnetized *Lonicera japonica* flower biomass for the sorption removal of heavy metals. *Hydrometallurgy* **165**, 81–89 (2016).
33. Threepanich, A. & Praipipat, P. Powdered and beaded lemon peels-doped iron(III) oxide-hydroxide materials for lead removal applications: Synthesis, characterizations, and lead adsorption studies. *J. Environ. Chem. Eng.* **9**, 106007 (2021).
34. Fan, S. *et al.* Preparation of sugarcane bagasse succinate/alginate porous gel beads via a self-assembly strategy: Improving the structural stability and adsorption efficiency for heavy metal ions. *Bioresour. Technol.* **306**, 123128 (2020).
35. Lakouraj, M. M., Mojerlou, F. & Zare, E. N. Nanogel and superparamagnetic nanocomposite based on sodium alginate for sorption of heavy metal ions. *Carbohydr. Polym.* **106**, 34–41 (2014).
36. Li, Y. *et al.* Controlled fabrication and characterization of α-FeOOH nanorods. *J. Inorg. Organomet. Polym. Mater.* **32**, 1400–1408 (2022).
37. Praipipat, P., Ngamsurach, P., Kosumphan, S. & Mokkarat, J. Powdered and beaded sawdust materials modified iron(III) oxide-hydroxide for adsorption of lead(II) ion and reactive blue 4 dye. *Sci. Rep.* **13**, 531 (2023).
38. Ngamsurach, P., Namwongsa, N. & Praipipat, P. Synthesis of powdered and beaded chitosan materials modified with ZnO for removing lead(II) ions. *Sci. Rep.* **12**, 17184 (2022).
39. Praipipat, P., Ngamsurach, P., Thanyahan, A. & Sakda, A. Reactive blue 4 adsorption efficiencies on bagasse and bagasse fly ash beads modified with titanium dioxide (TiO₂), magnesium oxide (MgO), and aluminum oxide (Al₂O₃). *Ind. Crop. Prod.* **191**, 115928 (2023).
40. Ngamsurach, P., Nemkhuntod, S., Chanaphan, P. & Praipipat, P. Modified beaded materials from recycled wastes of bagasse and bagasse fly ash with iron(III) oxide-hydroxide and zinc oxide for the removal of reactive blue 4 dye in aqueous solution. *ACS Omega* **7**, 34839–34857 (2022).
41. Praipipat, P., Ngamsurach, P., Saekrathok, C. & Phomtai, S. Chicken and duck eggshell beads modified with iron(III) oxide-hydroxide and zinc oxide for reactive blue 4 dye removal. *Arab. J. Chem.* **15**, 104291 (2022).
42. Liang, M. *et al.* Nano-hematite bagasse composite (*n*-HBC) for the removal of Pb(II) from dilute aqueous solutions. *J. Water Process Eng.* **21**, 69–76 (2018).
43. Hoang, M. T. *et al.* Esterification of sugarcane bagasse by citric acid for Pb²⁺ adsorption: Effect of different chemical pretreatment methods. *Environ. Sci. Pollut. Res.* **28**, 11869–11881 (2021).
44. Karnitz, O. *et al.* Adsorption of heavy metal ion from aqueous single metal solution by chemically modified sugarcane bagasse. *Bioresour. Technol.* **98**, 1291–1297 (2007).
45. Threepanich, A. & Praipipat, P. Efficacy study of recycling materials by lemon peels as novel lead adsorbents with comparing of material form effects and possibility of continuous flow experiment. *Environ. Sci. Pollut. Res.* **29**, 46077–46090 (2022).
46. Gurgel, L. V. A., de Freitas, R. P. & Gil, L. F. Adsorption of Cu(II), Cd(II), and Pb(II) from aqueous single metal solutions by sugarcane bagasse and mercerized sugarcane bagasse chemically modified with succinic anhydride. *Carbohydr. Polym.* **74**, 922–929 (2008).
47. Ngamsurach, P. & Praipipat, P. Modified alginate beads with ethanol extraction of *Cratogeomys formosum* and *Polygonum odoratum* for antibacterial activities. *ACS Omega* **6**, 32215–32230 (2021).
48. Ngamsurach, P. & Praipipat, P. Antibacterial activities against *Staphylococcus aureus* and *Escherichia coli* of extracted *Piper betle* leaf materials by disc diffusion assay and batch experiments. *RSC Adv.* **12**, 26435–26454 (2022).
49. Praipipat, P., Ngamsurach, P. & Prasongdee, V. Comparative reactive blue 4 dye removal by lemon peel bead doping with iron(III) oxide-hydroxide and zinc oxide. *ACS Omega* **7**, 41744–41758 (2022).
50. Ngamsurach, P. & Praipipat, P. Comparative antibacterial activities of *Garcinia cowa* and *Piper sarmentosum* extracts against *Staphylococcus aureus* and *Escherichia coli* with studying on disc diffusion assay, material characterizations, and batch experiments. *Heliyon* **8**, e11704 (2022).
51. Martín-Lara, M. Á., Rico, I. L. R., Vicente, I. D. L. C. A., García, G. B. & de Hoces, M. C. Modification of the sorptive characteristics of sugarcane bagasse for removing lead from aqueous solutions. *Desalination* **256**, 58–63 (2010).
52. Dos Santos, V. C. G., Gomes, C. A. T., Dragunski, D. C., Koslowski, L. A. D. & Lunelli, K. Removal of metals ions from aqueous solution using modified sugarcane bagasse. *Rev. Virtual Quim.* **11**, 1289–1301 (2019).
53. Malool, M. E., Keshavarz Moraveji, M. & Shayegan, J. Optimized production, Pb(II) adsorption and characterization of alkali modified hydrochar from sugarcane bagasse. *Sci. Rep.* **11**, 22328 (2021).
54. Liu, G. *et al.* Organic adsorbents modified with citric acid and Fe₃O₄ enhance the removal of Cd and Pb in contaminated solutions. *Chem. Eng. J.* **395**, 125108 (2020).
55. El Nemr, A. *et al.* New magnetic cellulose nanobiocomposites for Cu(II), Cd(II) and Pb(II) ions removal: Kinetics, thermodynamics and analytical evaluation. *Nanotechnol. Environ. Eng.* **6**, 1–20 (2021).
56. Ejaz, U. *et al.* Use of ionic liquid pretreated and fermented sugarcane bagasse as an adsorbent for Congo red removal. *Polymers (Basel)* **13**, 3943 (2021).

57. Langmuir, I. The adsorption of gases on plane surfaces of glass, mica and platinum. *J. Am. Chem. Soc.* **40**, 1361–1403 (1918).
58. Freundlich, H. Over the adsorption in solution. *J. Phys. Chem.* **57**, 385–470 (1906).
59. Temkin, M. I. & Pyzhev, V. Kinetics of ammonia synthesis on promoted iron catalysts. *Acta Physiochim. URSS* **12**, 327–356 (1940).
60. Dubinin, M. M. & Radushkevich, L. V. The equation of the characteristic curve of activated charcoal. *Proc. USSR Acad. Sci.* **55**, 327–329 (1947).
61. Jangkorn, S., Youngme, S. & Praipipat, P. Comparative lead adsorptions in synthetic wastewater by synthesized zeolite A of recycled industrial wastes from sugar factory and power plant. *Heliyon* **8**, e09323 (2022).
62. Lagergren, S. About the theory of so-called adsorption of soluble substances. *K. Sven. Vetenskapsakademiens Handl.* **24**, 1–39 (1898).
63. Ho, Y. S. & McKay, G. Pseudo-second order model for sorption processes. *Process Biochem.* **34**, 451–465 (1999).
64. Elovich, S. Y. & Larinov, O. G. Theory of adsorption from solutions of non electrolytes on solid (I) equation adsorption from solutions and the analysis of its simplest form, (II) verification of the equation of adsorption isotherm from solutions. *Izv. Akad. Nauk. SSSR Otd. Khim. Nauk* **2**, 209–216 (1962).
65. Weber, W. J. & Morris, J. C. Kinetics of adsorption carbon from solution. *J. Sanit. Eng. Div.* **89**, 31–60 (1963).

Acknowledgements

The authors are grateful for the financial support received from The Office of the Higher Education Commission and The Thailand Research Fund grant (MRG6080114), Coordinating Center for Thai Government Science and Technology Scholarship Students (CSTS) and National Science and Technology Development Agency (NSTDA) Fund grant (SCHNR2016-122), and Research and Technology Transfer Affairs of Khon Kaen University.

Author contributions

P.P.: Supervision, Conceptualization, Funding acquisition, Investigation, Methodology, Validation, Formal analysis, Visualization, Writing—Original Draft, Writing—Review and Editing. P.N.: Investigation, Visualization, Writing—Original Draft. A.S.: Investigation.

Competing interests

The authors declare no competing interests.

Additional information

Correspondence and requests for materials should be addressed to P.P.

Reprints and permissions information is available at www.nature.com/reprints.

Publisher's note Springer Nature remains neutral with regard to jurisdictional claims in published maps and institutional affiliations.



Open Access This article is licensed under a Creative Commons Attribution 4.0 International License, which permits use, sharing, adaptation, distribution and reproduction in any medium or format, as long as you give appropriate credit to the original author(s) and the source, provide a link to the Creative Commons licence, and indicate if changes were made. The images or other third party material in this article are included in the article's Creative Commons licence, unless indicated otherwise in a credit line to the material. If material is not included in the article's Creative Commons licence and your intended use is not permitted by statutory regulation or exceeds the permitted use, you will need to obtain permission directly from the copyright holder. To view a copy of this licence, visit <http://creativecommons.org/licenses/by/4.0/>.

© The Author(s) 2023